Math. Model. Nat. Phenom. 21 (2026) 22
https://doi.org/10.1051/mmnp/2026014

Mathematical Modelling of Natural Phenomena
www.mmnp-journal.org

MAGNETIC HÜCKEL THEORY: FRAMEWORK FOR THE HERMITIAN ADJACENCY MATRIX OF GRAPHS

Ernesto Estrada*

Abstract. We introduce a magnetic extension of the Hückel molecular orbital (HMO) method in which the effect of an external magnetic field is incorporated through the Peierls substitution. In this formulation, the π-electron Hamiltonian of a conjugated molecule becomes a complex-weighted hopping operator defined on the hydrogen-depleted molecular graph. Under the standard Hückel assumptions, the corresponding one-electron Hamiltonian matrix is proportional to the Hermitian adjacency matrix of the graph, providing a physical realization of Hermitian adjacency operators within molecular electronic structure theory. The magnetic-HMO framework enables the calculation of global flux-dependent observables such as orbital magnetization and orbital susceptibility from the magnetic adjacency spectrum, while local observables such as bond and ring currents are determined by the corresponding eigenvectors or one-particle density matrix. Applications to polycyclic aromatic hydrocarbons show that the magnetic response of π-electron systems is strongly controlled by molecular topology. In particular, linearly fused systems exhibit regular flux-dependent oscillations in the orbital magnetization, whereas nonlinear and extended molecules display more complex spectral rearrangements associated with multiple conjugation pathways.

Mathematics Subject Classification. 05C50, 92E10, 81Q10, 05C90.

Received February 25, 2026. Accepted June 18, 2026.

1. Introduction

The Hückel molecular orbital (HMO) method occupies a central place in the development of theoretical chemistry and spectral graph theory [1–5]. Originally introduced by Erich Hückel in 1931 [5] to describe π-electron systems in conjugated molecules, the HMO model provided one of the earliest and most successful connections between chemical structure and matrix spectra. In particular, the identification of the HMO Hamiltonian with the adjacency matrix of the hydrogen-depleted molecular graph established a direct correspondence between molecular electronic structure and graph eigenvalues [2–4].

Although the HMO Hamiltonian is formally similar to lattice Hamiltonians later used in condensed-matter physics, the tight-binding method was introduced independently several decades later as an approximation for electrons in crystalline solids [6]. In its modern form, tight-binding theory describes electron motion on a lattice in terms of hopping amplitudes between neighboring sites [7, 8], without explicit reference to Hückel's

Keywords and phrases: Hermitian graph operators, magnetic adjacency matrix, Peierls substitution, flux-dependent Hamiltonians.

Institute for Cross-Disciplinary Physics and Complex Systems (IFISC), CSIC-UIB, Palma de Mallorca, Spain.

* Corresponding author: estrada@ifisc.uib-csic.es

earlier molecular-orbital formulation. Thus, despite their similar matrix structure, Hückel theory and tight-binding theory originated in distinct physical contexts: the former in quantum chemistry for finite conjugated molecules, and the latter in condensed-matter physics for electrons in periodic lattices. By incorporating Peierls phase factors into the Hückel Hamiltonian, the magnetic-HMO model developed here combines a graph-based molecular analogue of magnetic tight-binding theory, connecting spectral graph models of conjugated molecules with lattice Hamiltonians used in orbital magnetism and flux-dependent electronic systems.

In recent years, growing attention has been devoted to magnetic or Hermitian extensions of graph operators, in particular to magnetic (Hermitian) graph Laplacians for directed or mixed graphs [9–14]. These operators arise naturally when complex phases are assigned to edges, corresponding to a discrete gauge field or magnetic connection on the graph. In this setting, the resulting Laplacian becomes a Hermitian operator whose spectrum depends on the magnetic fluxes associated with graph cycles.

Magnetic graph Laplacians have been studied from several perspectives, including discrete Schrödinger operators on graphs [14], spectral analysis of directed graphs [11], and signal processing and data analysis on networks [10]. Related constructions also appear in the theory of quantum walks, where complex edge weights encode phase accumulation along paths [15], and in the study of discrete gauge fields and magnetic networks [16]. These developments demonstrate that introducing complex phases into graph operators provides a natural way to model transport, circulation, and orientation effects on networks.

Ten years ago, Liu and Li [17] and Guo and Mohar [18] independently introduced a Hermitian adjacency matrix to study spectral properties of directed graphs. They showed, for instance, that eigenvalue interlacing properties hold for the eigenvalues of a digraph and its induced subdigraphs, and used this framework to define and study the energy of mixed graphs. Although some precedents exist in the work of Hoser and Geyer–Schulz [19], who defined Hermitian adjacency matrices to study social networks, the systematic spectral study of these matrices began with these works. Since then, Mohar has defined the so-called second–kind of Hermitian adjacency matrices [20], and many of their properties have been studied [21–32].

Despite this progress, an important conceptual gap remains. While the magnetic Laplacian has a clear physical motivation as the discrete Hamiltonian of a particle moving on a graph in the presence of a magnetic field [11, 14], the Hermitian adjacency matrix has so far lacked an equally direct physical realization in molecular electronic structure theory. Its introduction in spectral graph theory has been largely motivated by the representation and analysis of directed or mixed graphs, where complex phases encode edge orientation or flow information [17, 18]. However, such structures are uncommon in molecular sciences, where molecular graphs are typically undirected and encode chemical bonding connectivity rather than orientation. In particular, hydrogen-depleted molecular graphs arising in Hückel theory are simple undirected graphs, so the Hermitian adjacency matrix has not previously appeared as a natural operator in this context. Establishing a physical realization of this matrix within molecular electronic structure theory therefore remains an open conceptual problem.

In this work we introduce the magnetic Hückel molecular orbital method (magnetic HMO or m-HMO), an extension of the HMO approximation that incorporates the effect of an external magnetic field through the Peierls substitution [33]. Within this formulation, the π-electron Hamiltonian of a conjugated molecule becomes a complex-weighted hopping operator on the molecular graph. Our main result shows that, under the usual Hückel assumptions, the corresponding one-electron magnetic-HMO Hamiltonian is proportional to the Hermitian adjacency matrix of the hydrogen-depleted molecular graph. In this sense, magnetic Hückel theory provides a physical framework for Hermitian adjacency matrices, analogous to the role played by the standard HMO model for the ordinary adjacency matrix. We hope that placing the Hermitian adjacency matrix within the framework of magnetic Hückel theory will stimulate new interactions between spectral graph theory and quantum chemistry.

2. The magnetic-HMO method

Let a conjugated π-electron molecule be described within the Hückel molecular orbital (HMO) approximation [4]. After removing hydrogen atoms, the π-system can be represented by a graph $G = (V, E)$, called the hydrogen-depleted molecular graph, where $V = \{1, \ldots, n\}$ indexes the atomic p_z orbitals and $\{i, j\} \in E$ whenever orbitals i and j interact through a nearest-neighbour Hückel coupling.

In second quantization (spinless), the Hückel Hamiltonian is written as

$$\hat{H} = \sum_i \phi_i \, c_i^\dagger c_i + \sum_{\{i,j\} \in E} \left(t_{ij} \, c_i^\dagger c_j + t_{ij}^* \, c_j^\dagger c_i \right),$$

where $c_i^\dagger$ and c_i are the fermionic creation and annihilation operators associated with the p_z orbital at site i, ϕ_i is the on-site energy, and t_{ij} is the nearest-neighbour hopping amplitude between sites i and j. The second term is written explicitly in Hermitian form because the sum is taken over unordered edges $\{i, j\} \in E$.

To incorporate an external magnetic field, we apply the Peierls substitution [33, 34],

$$\hat{H}_m = \sum_i q\phi_i \, c_i^\dagger c_i + \sum_{\{i,j\} \in E} \left(t_{ij} \, \mathrm{e}^{i\theta_{ij}} \, c_i^\dagger c_j + t_{ij}^* \, \mathrm{e}^{-i\theta_{ij}} \, c_j^\dagger c_i \right),$$

where

$$\theta_{ij} = \frac{q}{\hbar} \chi_{ij}, \qquad \chi_{ij} = \int_{\mathbf{R}_j}^{\mathbf{R}_i} \mathbf{A}(\mathbf{r}) \cdot \mathrm{d}\mathbf{r},$$

$\mathbf{A}(\mathbf{r})$ is the magnetic vector potential, and $\mathbf{R}_i$ denotes the position of site i. The quantity θ_{ij} is dimensionless and represents the Peierls phase accumulated by an electron hopping from site j to site i in the presence of the magnetic field.

The Peierls phase depends on the direction of traversal of the bond. For each undirected edge $\{i, j\} \in E$, one may therefore introduce two oppositely oriented traversals (i, j) and (j, i) satisfying

$$\chi_{ji} = -\chi_{ij}, \qquad \theta_{ji} = -\theta_{ij}.$$

This auxiliary orientation does not modify the underlying molecular graph; it only specifies the direction used to evaluate the Peierls phase. The resulting phase assignment defines a discrete gauge field on the graph, and the relation $\theta_{ji} = -\theta_{ij}$ guarantees that the magnetic-Hückel Hamiltonian is Hermitian.

We now restrict to the usual simplified Hückel assumptions

$$\phi_i = 0, \qquad t_{ij} = -1 \qquad (\forall i, \ \{i, j\} \in E).$$

Let

$$\mathcal{H}_1 = \mathrm{span}\{|i\rangle\}_{i \in V}$$

denote the one-electron subspace, where

$$|i\rangle = c_i^\dagger |0\rangle.$$

In this basis,

$$\langle i | c_k^\dagger c_\ell | j \rangle = \delta_{ik} \delta_{\ell j},$$

so that

$$\langle i|\hat{H}_m|j\rangle = \begin{cases} -\,\mathrm{e}^{i\theta_{ij}}, & \{i,j\} \in E, \\ 0, & \text{otherwise.} \end{cases}$$

Remark 2.1. The Hamiltonian $\hat{H}_m$ obtained through the Peierls substitution is formally equivalent to magnetic tight-binding Hamiltonians used in condensed-matter physics to describe electrons on lattices in the presence of a magnetic field. In those models, complex hopping amplitudes encode the magnetic vector potential through Peierls phase factors $\mathrm{e}^{i\theta_{ij}}$, ensuring gauge invariance of the lattice Hamiltonian [33, 34]. Similar constructions appear in the theory of persistent currents in mesoscopic rings and in lattice models of orbital magnetism.

The magnetic-HMO method introduced here adopts a different physical context. Instead of modeling electrons in a crystalline lattice or metallic ring, the Hamiltonian is defined on the hydrogen-depleted molecular graph of a conjugated π-electron system. The vertices correspond to atomic p_z orbitals and the edges represent nearest-neighbour π interactions, so that the magnetic phases describe the response of a finite molecular π-electron network to an external magnetic field. In this sense, the magnetic-HMO approach may be viewed as a molecular-graph analogue of magnetic tight-binding theory, adapted to conjugated hydrocarbons within the HMO approximation.

Proposition 2.2. *[Magnetic adjacency representation] Let $G = (V, E)$ be the hydrogen-depleted molecular graph. For each edge $\{i, j\} \in E$, choose an arbitrary orientation (i, j) and assign a dimensionless Peierls phase $\theta_{ij} \in \mathbb{R}$ such that*

$$\theta_{ij} = \frac{q}{\hbar}\chi_{ij}, \qquad \theta_{ji} = -\theta_{ij}.$$

Define the matrix $\mathcal{A} \in \mathbb{C}^{n\times n}$ by

$$\mathcal{A}(i,j) = \begin{cases} \mathrm{e}^{i\theta_{ij}}, & \{i,j\} \in E, \\ 0, & \textit{otherwise.} \end{cases}$$

Then, in the one-electron basis $\{|i\rangle\}$,

$$\langle i|\hat{H}_m|j\rangle = -\,\mathcal{A}(i,j).$$

Equivalently, the one-electron magnetic-Hückel Hamiltonian matrix satisfies

$$H_m = -\,\mathcal{A}.$$

More generally, if the nearest-neighbour hopping amplitude is a real constant t, then

$$H_m = t\,\mathcal{A}.$$

In particular, $\mathcal{A}$ is Hermitian and may be interpreted as the magnetic adjacency matrix of the molecular graph.

Proof. From the matrix-element calculation above,

$$\langle i|\hat{H}_m|j\rangle = -\,\mathrm{e}^{i\theta_{ij}} \qquad \text{for } \{i,j\} \in E.$$

Therefore,

$$\langle i|\hat{H}_m|j\rangle = -\mathcal{A}(i,j),$$

which proves that

$$H_m = -\mathcal{A}$$

under the simplified Hückel choice $t_{ij} = -1$.

More generally, if the hopping amplitude is $t \in \mathbb{R}$, then

$$\langle i|\hat{H}_m|j\rangle = t\,\mathrm{e}^{i\theta_{ij}} = t\,\mathcal{A}(i,j),$$

so that

$$H_m = t\,\mathcal{A}.$$

Since

$$\theta_{ji} = -\theta_{ij},$$

one has

$$\mathcal{A}(j,i) = \mathrm{e}^{i\theta_{ji}} = \mathrm{e}^{-i\theta_{ij}} = \overline{\mathcal{A}(i,j)},$$

showing that $\mathcal{A}$ is Hermitian. □

Corollary 2.3 (Constant-phase Hermitian adjacency matrices)**.** *Let $G = (V,E)$ be the hydrogen-depleted molecular graph and let $\mathcal{A}$ be the magnetic adjacency matrix defined in Proposition 2.2. If the Peierls phases are chosen to be constant along all oriented edges,*

$$\theta_{ij} = \theta, \qquad \theta_{ji} = -\theta,$$

then $\mathcal{A}$ reduces to a Hermitian adjacency matrix with uniform phase factors

$$\mathcal{A}(i,j) = \begin{cases} \mathrm{e}^{i\theta}, & (i,j) \in E \textit{ with chosen orientation},\\ \mathrm{e}^{-i\theta}, & (j,i) \in E,\\ 0, & \textit{otherwise}. \end{cases}$$

In particular:

For $\theta = \pi/2$, one obtains the Hermitian adjacency matrix with entries i and $-i$ used for directed graphs in spectral graph theory [17, 18].

For $\theta = \pi/3$, one obtains the second-class Hermitian adjacency matrix of Mohar [20] with entries

$$\frac{1+i\sqrt{3}}{2}, \qquad \frac{1-i\sqrt{3}}{2}.$$

Thus, these Hermitian adjacency matrices may be interpreted as special cases of the magnetic-HMO Hamiltonian corresponding to tight-binding models with a uniform Peierls phase assigned to each bond.

However, unlike the magnetic-HMO construction derived from a vector potential, such constant-phase assignments do not generally correspond to a flux-consistent magnetic field determined by the molecular geometry.

Example 2.4. (Benzene in a perpendicular magnetic field). Consider benzene modeled as a six-site π-system forming the cycle graph C_6 in the xy-plane. A uniform magnetic field $\mathbf{B} = B\,\hat{\mathbf{z}}$ is applied perpendicular to the molecular plane. Let ℓ denote the C–C bond length. The six sites are placed at the vertices of a regular hexagon,

$$\mathbf{R}_k = \ell(\cos\theta_k, \sin\theta_k, 0), \qquad \theta_k = \frac{2\pi}{6}(k-1), \qquad k = 1, \ldots, 6.$$

Using the symmetric gauge

$$\mathbf{A}(\mathbf{r}) = \frac{1}{2}\mathbf{B} \times \mathbf{r},$$

the Peierls line integral along a nearest-neighbor bond can be evaluated explicitly and is the same for every bond:

$$\chi = \frac{\sqrt{3}}{4}\,B\ell^2.$$

If Φ denotes the magnetic flux through the hexagon, with

$$S = \frac{3\sqrt{3}}{2}\ell^2, \qquad \Phi = BS,$$

then the gauge-invariant phase accumulated around the ring is

$$\frac{q\Phi}{\hbar}.$$

By symmetry, this phase is uniformly distributed over the six bonds. Defining the dimensionless Peierls bond phase

$$\varphi = \frac{q}{\hbar}\chi,$$

we obtain

$$\varphi = \frac{1}{6}\frac{q\Phi}{\hbar}.$$

Equivalently, introducing the flux quantum

$$\Phi_0 = \frac{h}{|q|}, \qquad f = \frac{\Phi}{\Phi_0},$$

one may write

$$\varphi = \frac{2\pi}{6}\,\mathrm{sgn}(q)\,f.$$

Choosing the cycle orientation $1 \to 2 \to 3 \to 4 \to 5 \to 6 \to 1$, the magnetic adjacency matrix of benzene is

$$\mathcal{A}_{k,k+1} = \mathrm{e}^{i\varphi}, \qquad \mathcal{A}_{k+1,k} = \mathrm{e}^{-i\varphi}, \qquad \mathcal{A}_{kk} = 0,$$

with indices taken modulo 6. Explicitly,

$$\mathcal{A} = \begin{pmatrix} 0 & \mathrm{e}^{i\varphi} & 0 & 0 & 0 & \mathrm{e}^{-i\varphi} \\ \mathrm{e}^{-i\varphi} & 0 & \mathrm{e}^{\mathrm{i}\varphi} & 0 & 0 & 0 \\ 0 & \mathrm{e}^{-i\varphi} & 0 & \mathrm{e}^{\mathrm{i}\varphi} & 0 & 0 \\ 0 & 0 & \mathrm{e}^{-i\varphi} & 0 & \mathrm{e}^{\mathrm{i}\varphi} & 0 \\ 0 & 0 & 0 & \mathrm{e}^{-i\varphi} & 0 & \mathrm{e}^{\mathrm{i}\varphi} \\ \mathrm{e}^{\mathrm{i}\varphi} & 0 & 0 & 0 & \mathrm{e}^{-i\varphi} & 0 \end{pmatrix}.$$

The orientation used in the cycle $1 \to 2 \to 3 \to 4 \to 5 \to 6 \to 1$ is a reference traversal of the ring, not a physical orientation of chemical bonds. Each bond acquires the same Peierls phase when traversed along this direction, while the reverse traversal carries the opposite phase. This ensures that the total phase accumulated around the cycle equals $q\Phi/\hbar$, as required by gauge invariance.

This example illustrates the constant-phase situation described in the preceding corollary. In particular, specific values of the magnetic flux produce Hermitian adjacency matrices that coincide with well-known constructions in spectral graph theory.

If $\varphi = \pi/2$, then

$$\mathcal{A}_{k,k+1} = i, \qquad \mathcal{A}_{k+1,k} = -i,$$

which reproduces the Hermitian adjacency matrix with entries i and $-i$ used for oriented graphs [17, 18].

If $\varphi = \pi/3$, then

$$\mathcal{A}_{k,k+1} = \mathrm{e}^{\mathrm{i}\pi/3} = \frac{1 + i\sqrt{3}}{2}, \qquad \mathcal{A}_{k+1,k} = \mathrm{e}^{-i\pi/3} = \frac{1 - i\sqrt{3}}{2},$$

which yields the second-class Hermitian adjacency matrix introduced by Guo and Mohar [20].

Thus, the magnetic-HMO Hamiltonian for benzene provides a physical realization of these Hermitian adjacency matrices as special cases corresponding to uniform Peierls phases along the molecular cycle.

The precise relation between the magnetic adjacency matrix and the tight-binding Hamiltonian matrix H depends on the hopping-sign convention. If the Hückel nearest-neighbor hopping is chosen as $t_{ij} = -1$, then

$$H_{k,k+1} = -\mathrm{e}^{\mathrm{i}\varphi}, \qquad H_{k+1,k} = -\mathrm{e}^{-i\varphi},$$

so that

$$H = -\mathcal{A}.$$

More generally, if the real nearest-neighbor hopping amplitude is t (often $t < 0$ in Hückel notation), then

$$H_{k,k+1} = t\,\mathrm{e}^{\mathrm{i}\varphi}, \qquad H_{k+1,k} = t\,\mathrm{e}^{-i\varphi}.$$

A convenient dimensionless Hamiltonian is obtained by measuring energies in units of $|t|$:

$$\widetilde{H} = \frac{1}{|t|} H.$$

In this form, the Hamiltonian depends on the magnetic field only through the reduced flux

$$f = \frac{\Phi}{\Phi_0},$$

or equivalently through the bond phase

$$\varphi = \pm\frac{2\pi}{6}\,f.$$

3. Global observables

Throughout, the molecules are assumed to be planar, with one p_z orbital per carbon atom, nearest-neighbor hopping only, and uniform on-site energies. We now define global observables associated with the magnetic-HMO model. For a nearest-neighbour π-system, the magnetic Hückel Hamiltonian introduced in Section 2 may be written as

$$\hat{H}_m(\Phi) = \sum_{\{i,j\}\in E} t\,\mathrm{e}^{\mathrm{i}\varphi_{ij}(\Phi)}\,c_i^{\dagger}c_j + \mathrm{h.c.},$$

where $t < 0$ is the real nearest-neighbour hopping integral and $\varphi_{ij}(\Phi)$ are Peierls phases generated by a magnetic flux Φ threading the faces of the molecular graph.

Using the magnetic adjacency matrix $\mathcal{A}(\Phi)$ defined in Proposition 2.2, the Hamiltonian can be written equivalently as

$$\hat{H}_m(\Phi) = t\,\mathcal{A}(\Phi) \quad \text{(one-electron representation)}.$$

The reduced magnetic flux is defined as

$$f = \frac{\Phi}{\Phi_0}, \qquad \Phi_0 = \frac{h}{|q|},$$

and all magnetic-field dependence enters through $\mathcal{A}(\Phi)$.

Let

$$\mathcal{A}(\Phi)\,u_n(\Phi) = \lambda_n(\Phi)\,u_n(\Phi), \qquad n = 1,\ldots,n,$$

denote the eigenvalue problem for the magnetic adjacency matrix. Since $\mathcal{A}(\Phi)$ is Hermitian, the eigenvalues $\lambda_n(\Phi) \in \mathbb{R}$ and the eigenvectors $\{u_n(\Phi)\}$ form an orthonormal basis of $\mathbb{C}^n$.

Because $\hat{H}_m(\Phi) = t\,\mathcal{A}(\Phi)$, the single-particle Hamiltonian spectrum is obtained directly from the adjacency spectrum:

$$E_n(\Phi) = t\,\lambda_n(\Phi), \qquad \psi_n(\Phi) = u_n(\Phi).$$

Diagonalization of $\hat{H}_m(\Phi)$ therefore reduces to diagonalizing $\mathcal{A}(\Phi)$. The spectra of $\mathcal{A}(\Phi)$ for $\theta = \pi/2$ were previously studied by Liu and Li [17], as well as by Guo and Mohar [18], and for $\varphi = \pi/3$ by Mohar [20].

3.1. Magnetic graph energy

One of the most influential developments emerging from this connection is the concept of the energy of a graph, introduced by Gutman [35, 36] as a graph-theoretical analogue of the HMO π-electron energy. Graph energy is defined as the sum of the absolute values of the eigenvalues of the adjacency matrix and has become a central topic in chemical graph theory and spectral graph theory, with numerous mathematical results and applications [35, 36]. This line of research has stimulated extensive work on spectral invariants of molecular graphs and their chemical interpretation. More recently, the conceptual foundations of graph energy and its relation to matrix functions and network measures have been revisited from a broader spectral perspective [37]. We recall that the energy of Hermitian adjacency matrices has been previously studied by [17] for $\theta = \pi/2$. The many-electron ground-state energy is defined as

$$E_{\mathrm{GS}}(\Phi) = \sum_n g_n\, E_n(\Phi),$$

where g_n are the occupation numbers of the π orbitals. For closed-shell systems, $g_n = 2$ for occupied orbitals and $g_n = 0$ otherwise.

Using $E_n(\Phi) = t\,\lambda_n(\Phi)$, this can be written equivalently as

$$E_{\mathrm{GS}}(\Phi) = t\sum_n g_n\, \lambda_n(\Phi).$$

At $f = 0$, this reduces to the standard Hückel π-electron energy [4].

We now prove the following result about the stability of aromatic ($n = 4k + 2$ vertices, $k = 1, 2, \dots$) and antiaromatic ($n = 4k$ vertices, $k = 1, 2, \dots$) cycles in the presence of external magnetic field in relation to the absence of it.

Theorem 3.1. *Let $G = C_n$ be the cycle graph with n even. Fix an orientation*

$$1 \to 2 \to \cdots \to n \to 1$$

and define the magnetic adjacency matrix $\mathcal{A}(\varphi)$ by

$$\mathcal{A}(\varphi)_{k,k+1} = \mathrm{e}^{\mathrm{i}\varphi}, \qquad \mathcal{A}(\varphi)_{k+1,k} = \mathrm{e}^{-i\varphi}, \qquad (k \bmod n),$$

with all other off-diagonal entries zero and $\mathcal{A}_{kk} = 0$.

Let the one-electron magnetic-HMO Hamiltonian be

$$H(\varphi) = t\,\mathcal{A}(\varphi), \qquad t < 0.$$

At half-filling with spin ($N = n$ electrons), the closed-shell ground-state energy is

$$E_{\mathrm{GS}}(\varphi) = 2\sum_{m=1}^{n/2} E_m(\varphi),$$

where

$$E_1(\varphi) \le \cdots \le E_n(\varphi)$$

are the eigenvalues of $H(\varphi)$.

Define

$$S_n(\varphi) = \sum_{m=0}^{n-1} \left|\cos\!\left(\varphi + \frac{2\pi m}{n}\right)\right|.$$

Then:
If $n \equiv 2 \pmod 4$ *(aromatic case), then*

$$E_{\mathrm{GS}}(\varphi) \geq E_{\mathrm{GS}}(0) \qquad \textit{for all } \varphi \in \mathbb{R},$$

equivalently,

$$S_n(\varphi) \leq S_n(0).$$

Equality holds whenever

$$\varphi \equiv 0 \pmod{\frac{2\pi}{n}}.$$

If $n \equiv 0 \pmod 4$ *(antiaromatic case), then*

$$E_{\mathrm{GS}}(\varphi) \leq E_{\mathrm{GS}}(0) \qquad \textit{for all } \varphi \in \mathbb{R},$$

equivalently,

$$S_n(\varphi) \geq S_n(0).$$

Equality holds at discrete values of φ *for which the shifted sampling grid again contains zeros of* cos.
Equivalently, the energy shift

$$\Delta E(\varphi) = E_{\mathrm{GS}}(\varphi) - E_{\mathrm{GS}}(0)$$

is sign-definite:

$$\Delta E(\varphi) \geq 0 \quad \textit{for } n = 4k+2,$$

and

$$\Delta E(\varphi) \leq 0 \quad \textit{for } n = 4k.$$

Proof. The discrete Fourier modes diagonalize $\mathcal{A}(\varphi)$, giving

$$\lambda_m(\varphi) = 2\cos\left(\varphi + \frac{2\pi m}{n}\right), \qquad m = 0, 1, \ldots, n-1.$$

Hence the one-electron energies are

$$E_m(\varphi) = t\,\lambda_m(\varphi) = 2t\cos\left(\varphi + \frac{2\pi m}{n}\right).$$

Because C_n is bipartite for even n, the spectrum is symmetric: if λ is an eigenvalue then so is $-\lambda$. Therefore, at half-filling,

$$E_{\mathrm{GS}}(\varphi) = t\sum_{m=0}^{n-1} |\lambda_m(\varphi)| = 2t\,S_n(\varphi).$$

Since $t < 0$, comparing $E_{\mathrm{GS}}(\varphi)$ is equivalent to comparing $S_n(\varphi)$:

$$E_{\mathrm{GS}}(\varphi) \geq E_{\mathrm{GS}}(0) \iff S_n(\varphi) \leq S_n(0),$$

and

$$E_{\mathrm{GS}}(\varphi) \leq E_{\mathrm{GS}}(0) \iff S_n(\varphi) \geq S_n(0).$$

The function

$$g(x) = |\cos x|$$

is even and π-periodic. Moreover,

$$S_n\left(\varphi + \frac{2\pi}{n}\right) = S_n(\varphi),$$

because shifting φ by $2\pi/n$ only permutes the sampling points. Hence it suffices to consider

$$\varphi \in \left[0, \frac{\pi}{n}\right].$$

Case (a): $n = 4k + 2$.
At $\varphi = 0$, none of the sampling points

$$\frac{2\pi m}{n}$$

coincide with zeros of cos, since

$$\frac{2\pi m}{4k+2} = \frac{\pi}{2}$$

would imply

$$4m = 2k + 1,$$

which is impossible. Thus all terms contributing to $S_n(0)$ are strictly positive.
As φ moves away from 0, the equally spaced sampling grid shifts uniformly toward the zeros of $|\cos|$, decreasing the total sum. Therefore,

$$S_n(\varphi) \leq S_n(0).$$

Equality occurs precisely when the shifted grid coincides with the original one modulo π, namely when

$$\varphi \equiv 0 \pmod{\frac{2\pi}{n}}.$$

Since $t < 0$, this implies

$$E_{\mathrm{GS}}(\varphi) \geq E_{\mathrm{GS}}(0).$$

Case (b): $n = 4k$.

At $\varphi = 0$, the grid contains zeros of cos:

$$\cos\left(\frac{2\pi k}{n}\right) = \cos\left(\frac{\pi}{2}\right) = 0.$$

Hence $S_n(0)$ contains vanishing terms.

Any nonzero shift of the sampling grid moves these points away from the zeros and makes their contributions positive. Therefore,

$$S_n(\varphi) \geq S_n(0),$$

with equality only at discrete shifts for which the grid again contains zeros of cos.

Since $t < 0$, this gives

$$E_{\mathrm{GS}}(\varphi) \leq E_{\mathrm{GS}}(0).$$

This completes the proof. □

Remark 3.2 (Interpretation: Hückel aromaticity criterion from flux response)**.** For a single ring (annulene) at half-filling, the sign of $\Delta E(\varphi) = E_{\mathrm{GS}}(\varphi) - E_{\mathrm{GS}}(0)$ is fixed by $n \pmod 4$. In the aromatic case $n = 4k + 2$, zero flux gives the most stabilizing (most negative) closed-shell π-electron energy, and any applied flux raises the energy (diamagnetic response). In the antiaromatic case $n = 4k$, the zero-flux spectrum contains Fermi-level degeneracies (zeros of $|\cos|$), and flux lifts these degeneracies in a way that lowers the closed-shell energy (paramagnetic response). Thus, within the magnetic-HMO model for a single cycle, the $4k + 2/4k$ rule is equivalent to a sign-definite ordering of the half-filled band energy under flux.

A consequence of the previous Theorem is the following Corollary.

Corollary 3.3 (Absence of a universal energy ordering)**.** *There is no sign-definite inequality comparing the HMO ground-state energy $E_{\mathrm{GS}}(0)$ and the magnetic-HMO energy $E_{\mathrm{GS}}(\Phi)$ that holds for all conjugated π-systems.*

In particular, within the family of cycle graphs C_n at half-filling, $E_{\mathrm{GS}}(\Phi) > E_{\mathrm{GS}}(0)$ for aromatic rings ($n = 4k + 2$), whereas $E_{\mathrm{GS}}(\Phi) < E_{\mathrm{GS}}(0)$ for antiaromatic rings ($n = 4k$), for nonzero magnetic flux.

Example 3.4. Figure 1 compares the magnetic-HMO ground-state energy of anthracene and phenanthrene as a function of the reduced flux $f = \Phi/\Phi_0$, together with the evolution of their single-particle spectra. For all flux values in the interval $0 \leq f \leq 1$, the ground-state energy of anthracene remains higher than that of phenanthrene, indicating that the angular fusion of rings in phenanthrene leads to a more stabilizing π-electron delocalization under magnetic perturbation than the linear fusion present in anthracene.

The difference between the total energies is smallest at intermediate flux values (around $f \approx 0.35$ and $f \approx 0.65$), where the magnetic reorganization of the spectra in the two molecules becomes similar. In contrast, the largest difference occurs near half a flux quantum ($f = 1/2$), where anthracene exhibits a pronounced increase in ground-state energy.

This behavior can be understood from the flux dependence of the molecular orbital spectrum. At $f = 1/2$, several eigenvalues of the magnetic adjacency matrix for anthracene become pairwise degenerate, as visible in panel (b), reflecting enhanced symmetry of the effective hopping phases along the linear chain of fused hexagons. These degeneracies reduce the dispersion of the occupied levels and raise the total energy. In phenanthrene, shown in panel (c), the angular connectivity of the fused hexagons prevents the same degree of spectral pairing, and the occupied eigenvalues remain more separated. As a result, the total ground-state energy varies more smoothly with flux and does not exhibit the pronounced maximum observed in anthracene.

Overall, these results illustrate how the magnetic-HMO method captures the interplay between molecular topology and magnetic flux. Although anthracene and phenanthrene contain the same number of π electrons

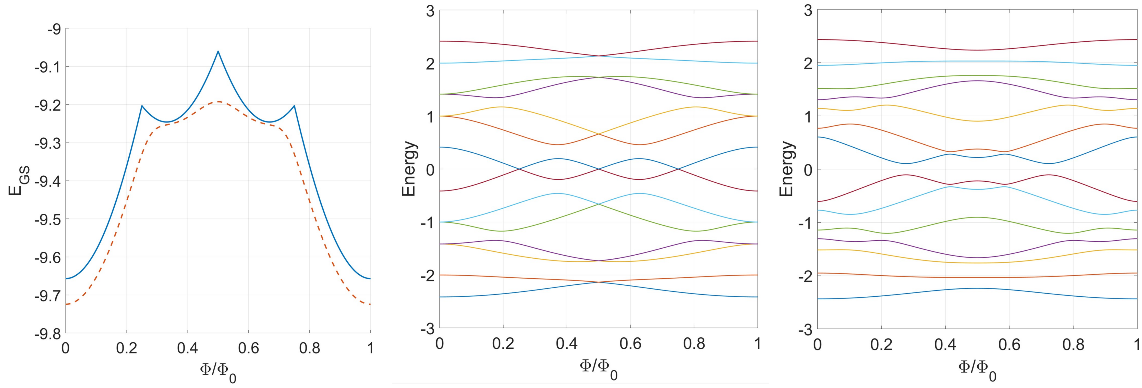

(A) (B) (C)

FIGURE 1. (a) Change of the total ground energy of anthracene (blue continuous curve) and phenanthrene (broken red curve) for different values of $f = \Phi/\Phi_0$. Change of the different energy levels in anthracene (b) and in phenanthrene (c) with the change in $f = \Phi/\Phi_0$.

and hexagonal rings, their different graph connectivity leads to distinct flux-dependent spectral reorganizations and ground-state energies. The comparison demonstrates that magnetic perturbations provide a sensitive probe of topological differences in conjugated polycyclic systems.

3.2. Density of states in the magnetic-HMO models

In the zero-field Hückel model, the Hamiltonian is

$$\hat{H}_0 = t\,\mathcal{A}_0,$$

where $\mathcal{A}_0$ is the adjacency matrix of the molecular graph. Let $\lambda_n^{(0)}$ denote the eigenvalues of $\mathcal{A}_0$. Then

$$E_n^{(0)} = t\,\lambda_n^{(0)}.$$

The non-magnetic density of states (DOS) is represented using Gaussian broadening,

$$\rho_{\mathrm{HMO}}(E) = \sum_n \frac{1}{\eta\sqrt{2\pi}} \exp\left[-\frac{(E - t\lambda_n^{(0)})^2}{2\eta^2}\right].$$

In the magnetic Hückel model, let $\lambda_n(\Phi)$ denote the eigenvalues of $\mathcal{A}(\Phi)$. Since

$$E_n(\Phi) = t\,\lambda_n(\Phi),$$

the magnetic density of states becomes

$$\rho_{\mathrm{mHMO}}(E;\Phi) = \sum_n \frac{1}{\eta\sqrt{2\pi}} \exp\left[-\frac{(E - t\lambda_n(\Phi))^2}{2\eta^2}\right].$$

This formulation shows that all spectral observables in the magnetic-HMO method are determined by the spectrum of the magnetic adjacency matrix $\mathcal{A}(\Phi)$.

Proposition 3.5 (Flux-invariant normalization and spectral moment constraints for the DOS)**.** *Let $G = (V, E)$ be a simple molecular graph on n vertices with magnetic adjacency matrix $\mathcal{A}(\Phi)$, and let*

$$\lambda_1(\Phi), \ldots, \lambda_n(\Phi) \in \mathbb{R}$$

denote its eigenvalues. Define the Gaussian-broadened magnetic DOS

$$\rho_{\mathrm{mHMO}}(E; \Phi) = \sum_{k=1}^{n} \frac{1}{\eta\sqrt{2\pi}} \exp\left[-\frac{(E - t\lambda_k(\Phi))^2}{2\eta^2}\right], \qquad \eta > 0.$$

For every Φ,

$$\int_{-\infty}^{\infty} \rho_{\mathrm{mHMO}}(E; \Phi)\, dE = n,$$

and

$$\int_{-\infty}^{\infty} E\, \rho_{\mathrm{mHMO}}(E; \Phi)\, \mathrm{d}E = t \sum_{k=1}^{n} \lambda_k(\Phi) = t\, \mathrm{Tr}\, \mathcal{A}(\Phi) = 0.$$

For higher powers, the moments of the Gaussian-broadened DOS are not identical to the spectral moments of $\mathcal{A}(\Phi)$. Rather, for every integer $r \geq 0$,

$$\int_{-\infty}^{\infty} E^r \rho_{\mathrm{mHMO}}(E; \Phi)\, \mathrm{d}E = \sum_{k=1}^{n} \sum_{s=0}^{\lfloor r/2 \rfloor} \binom{r}{2s} (2s-1)!!\eta^{2s} \big(t\lambda_k(\Phi)\big)^{r-2s},$$

with the convention $(-1)!! = 1$.

In particular,

$$\int_{-\infty}^{\infty} E^2 \rho_{\mathrm{mHMO}}(E; \Phi)\, \mathrm{d}E = t^2 \mathrm{Tr}\, \mathcal{A}(\Phi)^2 + n\eta^2,$$

and

$$\int_{-\infty}^{\infty} E^3 \rho_{\mathrm{mHMO}}(E; \Phi)\, \mathrm{d}E = t^3 \mathrm{Tr}\, \mathcal{A}(\Phi)^3 + 3\eta^2 t\, \mathrm{Tr}\, \mathcal{A}(\Phi).$$

The discrete spectral moments themselves satisfy

$$\sum_{k=1}^{n} \lambda_k(\Phi)^m = \mathrm{Tr}\, \mathcal{A}(\Phi)^m.$$

Thus, the closed-walk interpretation applies directly to the discrete spectral moments of $\mathcal{A}(\Phi)$, or equivalently to the limiting DOS as $\eta \to 0$, but the Gaussian-broadened DOS moments contain additional η-dependent correction terms.

If G is bipartite, then $\mathcal{A}(\Phi)$ has a chiral symmetry – in standard tight-binding/condensed-matter sense, not in the chemical stereochemistry sense – and its spectrum is symmetric:

$$\{\lambda_k(\Phi)\}_{k=1}^{n} = \{-\lambda_k(\Phi)\}_{k=1}^{n} \quad \textit{as multisets.}$$

Consequently,

$$\operatorname{Tr} \mathcal{A}(\Phi)^{2r+1} = 0, \qquad r = 0, 1, 2, \dots.$$

Moreover, since the broadened DOS is obtained by placing identical Gaussian kernels at the symmetric energy levels $t\lambda_k(\Phi)$*, it is also symmetric:*

$$\rho_{\mathrm{mHMO}}(E;\Phi) = \rho_{\mathrm{mHMO}}(-E;\Phi).$$

Proof. Each Gaussian term integrates to 1, hence the total integral of the DOS is n. Its first moment is the sum of the Gaussian centers:

$$\int E\, \rho_{\mathrm{mHMO}}(E;\Phi)\, \mathrm{d}E = \sum_{k=1}^{n} t\lambda_k(\Phi) = t \operatorname{Tr} \mathcal{A}(\Phi) = 0,$$

because $\mathcal{A}(\Phi)$ has zero diagonal.

For the general broadened moment, write each Gaussian as the distribution of a random variable

$$E = t\lambda_k(\Phi) + X,$$

where X is a centered Gaussian random variable with variance η^2. Then

$$\mathbb{E}\big[(t\lambda_k + X)^r\big] = \sum_{s=0}^{\lfloor r/2 \rfloor} \binom{r}{2s} (t\lambda_k)^{r-2s} \mathbb{E}[X^{2s}],$$

and

$$\mathbb{E}[X^{2s}] = (2s-1)!!\, \eta^{2s}.$$

Summing over k gives the stated formula.

The identity

$$\sum_{k=1}^{n} \lambda_k(\Phi)^m = \operatorname{Tr} \mathcal{A}(\Phi)^m$$

is the usual spectral trace identity. Since $\mathcal{A}(\Phi)$ is supported on edges, the diagonal entries of $\mathcal{A}(\Phi)^m$ expand as sums over closed walks of length m, with each walk weighted by the product of the corresponding magnetic edge phases.

Finally, if G is bipartite with vertex partition $V = U \sqcup W$, then in the ordered basis (U, W),

$$\mathcal{A}(\Phi) = \begin{pmatrix} 0 & B \\ B^* & 0 \end{pmatrix}.$$

Let

$$J = \operatorname{diag}(I_{|U|}, -I_{|W|}).$$

Then

$$J\mathcal{A}(\Phi)J = -\mathcal{A}(\Phi),$$

which implies spectral symmetry. The vanishing of odd spectral moments follows immediately, and the symmetry of the broadened DOS follows by pairing the Gaussian centered at $t\lambda$ with the Gaussian centered at $-t\lambda$. $\square$

Remark 3.6. It is worth noticing here that powers of Hermitian adjacency matrices have been recently studied [38], as a way to count graph walks indexed by the number of edge reversals and establishing that walk profiles correspond to a Fourier transform of hermitian matrix powers.

Proposition 3.7 (First flux-sensitive spectral moment in benzenoids)**.** *Let G be a planar benzenoid graph and let $\mathcal{A}(\Phi)$ denote its magnetic adjacency matrix. Then the spectral moments*

$$\operatorname{Tr} \mathcal{A}(\Phi)^m$$

are independent of the magnetic flux for all $m < 6$. The first spectral moment that depends on the magnetic field is $m = 6$, corresponding to closed walks around hexagonal faces.

Proof. For any weighted adjacency matrix, the trace $\operatorname{Tr} \mathcal{A}(\Phi)^m$ admits a combinatorial interpretation as a sum over closed walks of length m, each weighted by the product of edge weights along the walk.

In the magnetic adjacency matrix, each oriented edge (i, j) carries a phase $\mathrm{e}^{\mathrm{i}\varphi_{ij}}$, with $\varphi_{ji} = -\varphi_{ij}$. Whenever a walk immediately retraces an edge, the corresponding phase factors cancel:

$$\mathrm{e}^{\mathrm{i}\varphi_{ij}}\mathrm{e}^{-i\varphi_{ij}} = 1.$$

Since the shortest cycles in a benzenoid graph have length 6, any closed walk of length $m < 6$ necessarily contains backtracking segments. Therefore, all phase factors cancel pairwise, and the trace is identical to the zero-field value:

$$\operatorname{Tr} \mathcal{A}(\Phi)^m = \operatorname{Tr} \mathcal{A}(0)^m, \qquad m < 6.$$

For $m = 6$, closed walks can traverse a hexagonal face without backtracking. The product of the phases along such a loop equals

$$\exp\left(i \sum_{(i,j)\in\partial\mathscr{F}} \varphi_{ij} \right) = \exp\left(i \frac{q\Phi_{\mathscr{F}}}{\hbar} \right),$$

where $\Phi_{\mathscr{F}}$ is the magnetic flux through the face $\mathscr{F}$. Hence $\operatorname{Tr} \mathcal{A}(\Phi)^6$ depends on the magnetic flux. $\square$

Example 3.8 (Spectral moment $m = 6$ for benzene)**.** Consider benzene modeled as the cycle graph C_6 with a uniform Peierls phase φ on each oriented bond. The eigenvalues of the magnetic adjacency matrix are

$$\lambda_k(\varphi) = 2\cos\left(\frac{2\pi k}{6} + \varphi \right), \qquad k = 0, \ldots, 5.$$

The sixth spectral moment is

$$\operatorname{Tr} \mathcal{A}(\varphi)^6 = \sum_{k=0}^{5} \lambda_k(\varphi)^6.$$

Using the identity

$$\cos^6 x = \frac{10 + 15\cos(2x) + 6\cos(4x) + \cos(6x)}{32},$$

one finds that all oscillatory terms cancel except the term involving $\cos(6\varphi)$. A direct computation yields

$$\operatorname{Tr} \mathcal{A}(\varphi)^6 = 120 + 12\cos(6\varphi).$$

Since the total phase accumulated around the hexagonal cycle is

$$6\varphi = \frac{q\Phi}{\hbar},$$

this can be written as

$$\operatorname{Tr} \mathcal{A}(\Phi)^6 = 120 + 12\cos\left(\frac{q\Phi}{\hbar}\right).$$

Equivalently, using the reduced flux

$$f = \frac{\Phi}{\Phi_0}, \qquad \Phi_0 = \frac{h}{|q|},$$

one obtains

$$\operatorname{Tr} \mathcal{A}(\Phi)^6 = 120 + 12\cos(2\pi f).$$

This explicitly shows that the first flux-dependent spectral moment corresponds to closed walks around the hexagonal ring.

In the magnetic-HMO model the density of states is explicitly flux-dependent, since the Peierls phases modify the hopping amplitudes and continuously reshape the molecular spectrum. In Figure 2, we illustrate the DOS of C_4 (cyclobutadiene), C_6 (benzene), and two fused hexagons (naphthalene) for different values of the reduced flux f.

Example 3.9. In the standard HMO description, the density of states (DOS) of cyclic π-systems reflects the degeneracy structure imposed by the symmetry of the molecular graph. For cyclobutadiene (C_4), the zero-field spectrum consists of one bonding level, one antibonding level, and a doubly degenerate pair of nonbonding orbitals at zero energy, producing three distinct peaks in the DOS. For benzene (C_6), the spectrum contains degenerate levels at $\pm\beta$ together with nondegenerate levels at $\pm 2\beta$, yielding four DOS peaks. In naphthalene, the larger molecular graph produces a richer spectrum with several degeneracies inherited from its bipartite structure and mirror symmetry.

When a magnetic flux is introduced through the Peierls substitution, time-reversal symmetry is broken and the allowed crystal-momentum values along cyclic paths in the molecular graph are continuously shifted. As a result, degeneracies in the HMO spectrum are lifted in a flux-dependent manner. At intermediate flux values (*e.g.* $f = 0.25$), the eigenvalues of the magnetic adjacency matrix typically become nondegenerate, and the DOS splits into a larger number of distinct peaks of comparable spectral weight. This behavior is clearly visible in C_4, C_6, and naphthalene, although the detailed pattern depends on the size and connectivity of the graph.

As the flux approaches half a flux quantum ($f = 1/2$), new degeneracies may appear due to the periodicity of the Aharonov–Bohm phase. In even-membered cycles such as C_4 and C_6, this produces a reorganization of

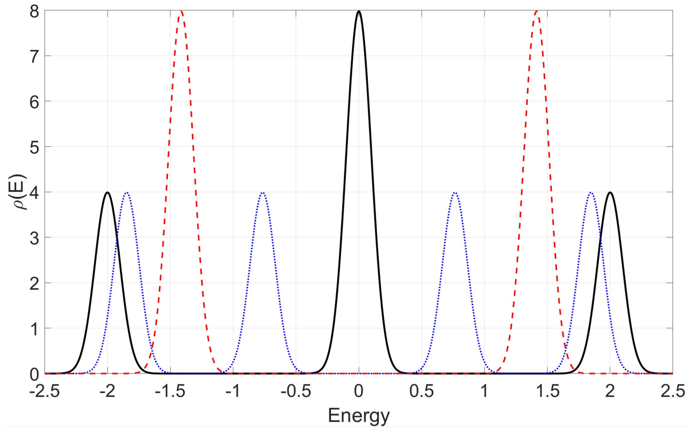

(A)

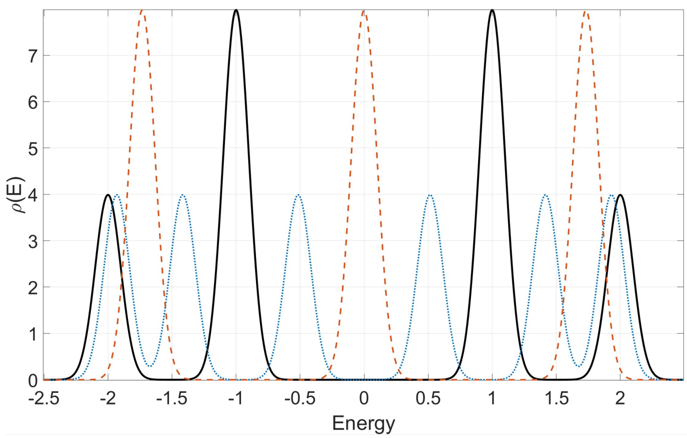

(B)

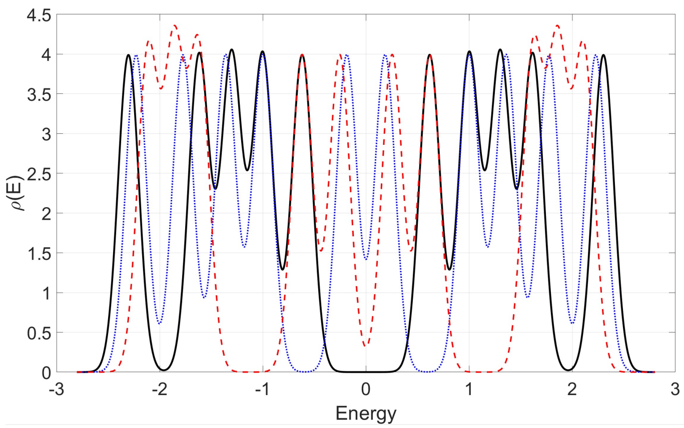

(C)

FIGURE 2. DOS of the cycle C_4 (cyclobutadiene molecule) (a), of C_6 (benzene molecule) (b) and of the bicyclic structure of two fused hexagons (naphthalene molecule) (c) showing the plots for the standard HMO (black continuous line), magnetic HMO with $f = 0.25$ (dotted blue line), and with $f = 0.5$ (broken red line).

the spectrum and the formation of symmetric energy pairs around zero energy. In particular, flux-induced level crossings may generate states at or near zero energy that correspond to circulating molecular orbitals whose kinetic energy is compensated by the magnetic phase. Similar reorganizations occur in naphthalene, where the presence of two fused hexagons leads to coupled ring currents and a redistribution of spectral weight among the molecular orbitals.

Overall, the DOS evolution from zero flux to half a flux quantum illustrates how magnetic flux redistributes electronic states in conjugated molecules by continuously reshaping orbital degeneracies. While the qualitative mechanism is common to cyclic and benzenoid systems, the detailed spectral response is controlled by the topology of the molecular graph and the number of hexagonal cycles through which the magnetic flux is threaded.

3.3. Orbital magnetization and flux-dependent susceptibility

The orbital magnetic response of the magnetic-HMO system can be characterized by the flux-dependent ground-state energy

$$E_{\mathrm{GS}}(f),$$

viewed as a function of the reduced flux

$$f = \frac{\Phi}{\Phi_0}.$$

From this quantity, the orbital magnetization and the flux-dependent orbital susceptibility are defined as

$$M(f) = -\frac{\mathrm{d}E_{\mathrm{GS}}}{\mathrm{d}f}, \qquad \chi(f) = -\frac{d^2 E_{\mathrm{GS}}}{\mathrm{d}f^2}.$$

Time-reversal symmetry enforces

$$M(0) = 0.$$

Using the spectral representation of the magnetic-HMO Hamiltonian,

$$E_{\mathrm{GS}}(\Phi) = \sum_n g_n E_n(\Phi), \qquad E_n(\Phi) = t\,\lambda_n(\Phi),$$

where $\lambda_n(\Phi)$ are the eigenvalues of the magnetic adjacency matrix $\mathcal{A}(\Phi)$, differentiation with respect to the reduced flux gives

$$M(f) = -\,t \sum_n \left[g_n \frac{\mathrm{d}\lambda_n(\Phi)}{\mathrm{d}f} + \lambda_n(\Phi) \frac{\mathrm{d}g_n}{\mathrm{d}f} \right].$$

Away from level crossings and changes in orbital occupation, the occupation numbers g_n are constant with respect to f, so that

$$\frac{\mathrm{d}g_n}{\mathrm{d}f} = 0.$$

In this regime,

$$M(f) = -t \sum_n g_n \frac{\mathrm{d}\lambda_n(\Phi)}{\mathrm{d}f}.$$

Thus, away from occupation rearrangements, the orbital magnetization is determined entirely by the flux dependence of the magnetic adjacency spectrum.

The orbital magnetization provides a direct measure of the net persistent current induced in the molecular ground state at finite magnetic flux. Unlike the magnetic susceptibility, which is fundamentally a zero-field linear-response quantity, the magnetization remains well defined at finite flux and captures nonlinear current-carrying regimes as well as flux-driven electronic rearrangements. Changes in slope or sign of $M(f)$ correlate with level crossings in the magnetic-HMO spectrum (equivalently, in the spectrum of $\mathcal{A}(\Phi)$) and signal reversals or suppression of circulating currents.

In the numerical calculations presented below, $M(f)$ and $\chi(f)$ are obtained from the flux-dependent eigenvalues of the magnetic-HMO Hamiltonian by numerical differentiation of $E_{\mathrm{GS}}(f)$. These observables depend ultimately on the flux-dependent eigenvectors of $\mathcal{A}(\Phi)$ (or equivalently on the density matrix $\gamma(\Phi)$), while their qualitative behavior is often controlled by changes in the magnetic-HMO spectrum, such as level crossings or degeneracy lifting.

A particularly important quantity is the orbital susceptibility at zero field,

$$\chi_0 = \chi(0) = -\left.\frac{d^2 E_{\mathrm{GS}}}{\mathrm{d}f^2}\right|_{f=0}.$$

When $E_{\mathrm{GS}}(f)$ is twice differentiable at $f = 0$, χ_0 can be estimated numerically by fitting the ground-state energy near $f = 0$ to a quadratic form,

$$E_{\mathrm{GS}}(f) \simeq af^2 + bf + c, \qquad \chi_0 = -2a.$$

For systems exhibiting a cusp at $f = 0$, such as antiaromatic $4k$ cycles, this quadratic approximation is not valid and no finite zero-field susceptibility is assigned without additional regularization.

Proposition 3.10 (Orbital magnetization and susceptibility)**.** *Let $E_{\mathrm{GS}}(f)$ be the closed-shell ground-state energy of the magnetic-HMO Hamiltonian, viewed as a function of the reduced flux $f = \Phi/\Phi_0$. Assume that $E_{\mathrm{GS}}(f)$ is twice differentiable at $f = 0$. Define*

$$M(f) = -\frac{\mathrm{d}E_{\mathrm{GS}}}{\mathrm{d}f}, \qquad \chi(f) = \frac{\mathrm{d}M}{\mathrm{d}f} = -\frac{d^2 E_{\mathrm{GS}}}{\mathrm{d}f^2}.$$

Then:

$$E_{\mathrm{GS}}(-f) = E_{\mathrm{GS}}(f),$$

that is, $E_{\mathrm{GS}}(f)$ is an even function of f.

The orbital magnetization $M(f)$ is an odd function of f, hence

$$M(0) = 0.$$

Near $f = 0$, the ground-state energy admits the expansion

$$E_{\mathrm{GS}}(f) = E_{\mathrm{GS}}(0) - \frac{\chi_0}{2} f^2 + o(f^2),$$

where

$$\chi_0 = \chi(0) = - \left. \frac{d^2 E_{\mathrm{GS}}}{\mathrm{d}f^2} \right|_{f=0}.$$

Consequently, if $E_{\mathrm{GS}}(f)$ has a local minimum at $f = 0$, then $\chi_0 < 0$, whereas if it has a local maximum at $f = 0$, then $\chi_0 > 0$.

Proof. Under time-reversal, the Peierls phases change sign,

$$\varphi_{ij}(f) \mapsto -\varphi_{ij}(f),$$

which corresponds to $f \mapsto -f$. Since the magnetic adjacency matrix satisfies

$$\mathcal{A}(-f) = \overline{\mathcal{A}(f)},$$

the Hamiltonians

$$H(-f) = t\,\mathcal{A}(-f) \qquad \text{and} \qquad H(f) = t\,\mathcal{A}(f)$$

are related by complex conjugation and therefore have identical spectra. Hence

$$E_{\mathrm{GS}}(-f) = E_{\mathrm{GS}}(f).$$

Differentiating this identity gives

$$M(-f) = -M(f),$$

so $M(f)$ is odd and therefore

$$M(0) = 0.$$

Since $E_{\mathrm{GS}}(f)$ is even and twice differentiable at $f = 0$, its Taylor expansion contains no linear term:

$$E_{\mathrm{GS}}(f) = E_{\mathrm{GS}}(0) + \frac{1}{2} E''_{\mathrm{GS}}(0) f^2 + o(f^2).$$

Using

$$\chi_0 = -E''_{\mathrm{GS}}(0),$$

we obtain

$$E_{\mathrm{GS}}(f) = E_{\mathrm{GS}}(0) - \frac{\chi_0}{2} f^2 + o(f^2).$$

□

Theorem 3.11. *Let $G = C_n$ be the cycle graph with n even, and let $\mathcal{A}(\varphi)$ be the magnetic adjacency matrix with uniform bond phase φ. Let*

$$H(\varphi) = t\,\mathcal{A}(\varphi), \qquad t < 0,$$

and consider half-filling with spin ($N = n$). Write

$$f = \frac{\Phi}{\Phi_0}, \qquad \varphi = \frac{2\pi}{n}\,\mathrm{sgn}(q)\,f.$$

Then $E_{\mathrm{GS}}(f)$ is even and Φ_0-periodic, and $M(f)$ is odd with $M(0) = 0$ whenever E_{GS} is differentiable at $f = 0$.

For $n = 4k + 2$ (aromatic case), $E_{\mathrm{GS}}(f)$ is smooth near $f = 0$ and has a local minimum at $f = 0$. Hence, with the convention

$$M(f) = -\frac{\mathrm{d}E_{\mathrm{GS}}}{\mathrm{d}f}, \qquad \chi(f) = \frac{\mathrm{d}M}{\mathrm{d}f} = -\frac{d^2E_{\mathrm{GS}}}{\mathrm{d}f^2},$$

one has

$$\chi(0) < 0,$$

corresponding to a diamagnetic response.

For $n = 4k$ (antiaromatic case), the Fermi-level degeneracy at $f = 0$ produces a cusp in $E_{\mathrm{GS}}(f)$. Thus $E''_{\mathrm{GS}}(0)$ does not exist in the ordinary sense, and no finite zero-field susceptibility $\chi(0)$ is assigned without an additional regularization. The leading nonanalytic decrease of $E_{\mathrm{GS}}(f)$ under infinitesimal flux corresponds to a paramagnetic tendency.

Proof. For C_n with uniform phase φ, the eigenvalues of $\mathcal{A}(\varphi)$ are

$$\lambda_m(\varphi) = 2\cos\left(\varphi + \frac{2\pi m}{n}\right), \qquad m = 0, \ldots, n-1.$$

At half-filling, the ground-state energy equals twice the sum of the lowest $n/2$ one-electron energies. Since C_n is bipartite for even n, the spectrum is symmetric about zero, yielding

$$E_{\mathrm{GS}}(\varphi) = 2t\sum_{m=0}^{n-1}\left|\cos\left(\varphi + \frac{2\pi m}{n}\right)\right|.$$

The evenness and periodicity follow from the symmetry and periodicity of the shifted sampling grid. The relation

$$\varphi = \frac{2\pi}{n}\,\mathrm{sgn}(q)\,f$$

transfers these properties to $E_{\mathrm{GS}}(f)$.

If $n = 4k + 2$, none of the sampled points coincides with a zero of the cosine at $f = 0$. Therefore the absolute-value terms are smooth near $f = 0$. By the preceding energy-ordering result, $E_{\mathrm{GS}}(f)$ has a local minimum at $f = 0$, so

$$E''_{\mathrm{GS}}(0) > 0.$$

With

$$\chi(0) = -E''_{\mathrm{GS}}(0),$$

this gives

$$\chi(0) < 0.$$

This is the diamagnetic case under the thermodynamic sign convention.

If $n = 4k$, the sampling grid contains zeros of the cosine at $f = 0$. The absolute-value terms associated with the Fermi-level states therefore generate a cusp in $E_{\mathrm{GS}}(f)$. Consequently, $E''_{\mathrm{GS}}(0)$ is not finite in the ordinary sense, and the zero-field susceptibility is not defined unless a regularization scheme is introduced. The cusp corresponds to the lowering of the energy under infinitesimal flux and hence to a paramagnetic tendency. □

Remark 3.12. [Interpretation] For a single ring at half-filling, the $4k+2/4k$ rule manifests not only in the sign of the energy shift under flux but also in the leading behavior of the orbital magnetization and susceptibility near $f = 0$.

Aromatic rings ($n = 4k + 2$) exhibit a smooth quadratic minimum of the ground-state energy at $f = 0$. Consequently, $\chi(0) < 0$, corresponding to a diamagnetic response under the convention adopted here. By contrast, antiaromatic rings ($n = 4k$) exhibit a cusp in $E_{\mathrm{GS}}(f)$ at $f = 0$ caused by the lifting of the Fermi-level degeneracy under infinitesimal flux. In this case the second derivative at $f = 0$ does not exist in the ordinary sense, so no finite zero-field susceptibility is assigned without additional regularization. The cusp nevertheless reflects a paramagnetic tendency.

Example 3.13. In Figure 3, we illustrate the orbital magnetization (left panel) and the flux-dependent orbital susceptibility (right panel) of anthracene and phenanthrene.

The magnetization $M(f)$ exhibits alternating negative and positive branches as a function of flux, indicating successive changes in the slope of the ground-state energy. These sign reversals and the associated local minima and maxima arise from flux-induced spectral rearrangements, including degeneracy lifting and avoided crossings in the magnetic-HMO eigenvalue spectrum. The extrema occur at different flux values for anthracene and phenanthrene, reflecting the distinct conjugation topologies of linear (anthracene) versus angular (phenanthrene) ring fusion.

Physically, these sign changes correspond to alternations in the direction and strength of the field-induced π-electron circulation, and therefore to changes in the orbital magnetic response of the molecule. Within the thermodynamic convention adopted here, negative values of $\chi(f)$ correspond to diamagnetic behavior, whereas positive values correspond to paramagnetic behavior.

The observed zigzag pattern therefore reflects a sequence of flux-driven redistributions of π-electron currents within the molecular framework, as different conjugation pathways become dominant at different flux values. These transitions are more localized in anthracene, where the response is largely governed by a perimeter circulation pathway, while in phenanthrene they are more broadly distributed due to the presence of competing conjugation routes in the angularly fused structure.

The flux-dependent orbital susceptibility $\chi(f)$ exhibits pronounced positive maxima at specific finite-flux values for both anthracene and phenanthrene. In anthracene, large maxima appear at $f \approx 0.25$, 0.50, and 0.75, with amplitudes of approximately 420, 405, and 420, respectively. In phenanthrene, analogous features are observed at $f \approx 0.275$, 0.50, and 0.725, with smaller amplitudes of about 81, 27, and 81. These positive finite-flux maxima correspond to regions where the ground-state energy $E_{\mathrm{GS}}(f)$ displays strong downward curvature. They should therefore be interpreted as local paramagnetic contributions arising at finite flux, while the negative values of $\chi(f)$ near $f = 0$ remain consistent with the diamagnetic zero-field response of these molecules.

Physically, the pronounced extrema in $\chi(f)$ signal flux values at which the π-electron system becomes particularly sensitive to magnetic perturbation due to flux-induced rearrangements in the magnetic-HMO spectrum. Near these flux values, small changes in f produce relatively large changes in the slope of $E_{\mathrm{GS}}(f)$. This behavior

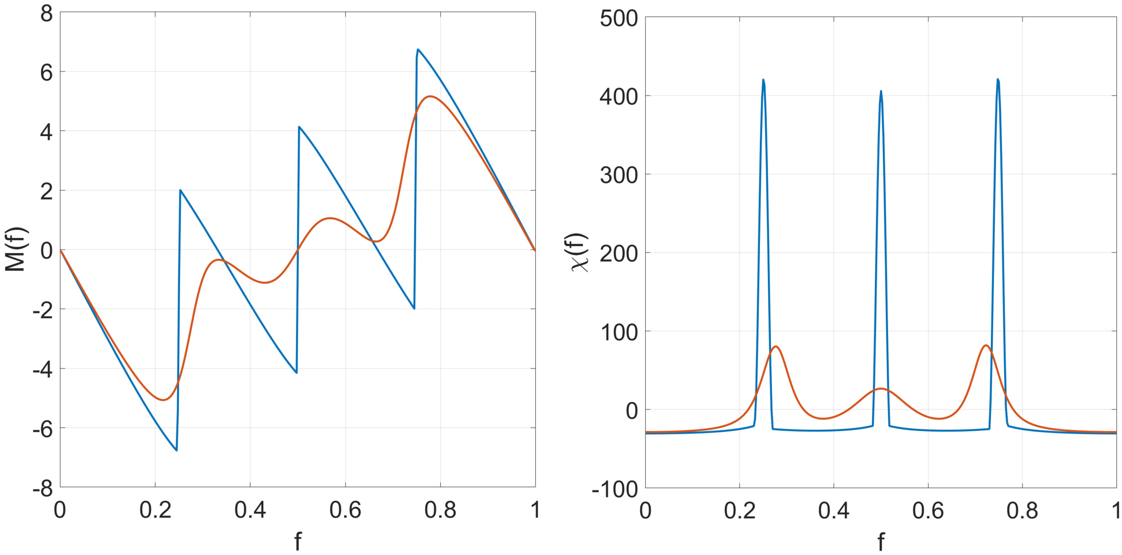

FIGURE 3. Change in the orbital magnetization (left panel) and the flux-dependent orbital susceptibility (right panel) of anthracene (blue curves) and phenanthrene (red curves) as a function of f.

is typically associated with avoided crossings or degeneracy lifting among molecular orbitals, where the magnetic field modifies the balance between competing conjugation pathways.

The difference in peak magnitude between anthracene and phenanthrene reflects their distinct topologies. In anthracene, the linear fusion of rings supports a dominant conjugation pathway along the molecular backbone, producing a stronger collective response of the π system to the magnetic flux and consequently larger susceptibility extrema in magnitude. In phenanthrene, the angular fusion introduces competing pathways for π-electron circulation, distributing the magnetic response more evenly across the molecule and leading to smaller susceptibility extrema. The approximate symmetry of the peaks around $f = 0.5$ in both molecules is consistent with the periodic and time-reversal symmetry properties of the magnetic-HMO Hamiltonian.

Remark 3.14. The oscillatory behavior observed in the flux-dependent orbital magnetization $M(f)$ and susceptibility $\chi(f)$ is reminiscent of magnetic-response oscillations arising from field-dependent spectral rearrangements in lattice-electron systems. In tight-binding models subject to Peierls phases, quantum oscillations of the orbital magnetization as a function of magnetic field have been reported even in the absence of conventional Landau-level physics, where the effect is driven by flux-dependent restructuring of the electronic spectrum [39].

In the present case, the effect arises from the flux dependence of the magnetic-HMO eigenvalues of a finite π-electron system rather than from Landau-level quantization in a bulk conductor. As the reduced flux varies, changes in the ordering and curvature of the occupied eigenvalues produce alternating diamagnetic and paramagnetic contributions to the orbital response, leading to the zigzag structure in $M(f)$ and the pronounced peaks in $\chi(f)$. Thus, the magnetic-HMO description predicts a finite-molecule analogue of flux-driven magnetization oscillations arising from spectral quantization in a Peierls-phase Hamiltonian defined on a molecular graph. We emphasize that this analogy is conceptual rather than literal: the oscillatory behavior reported here originates from flux-dependent rearrangements of discrete molecular π-electron energy levels, whereas oscillations in extended systems arise from magnetic-field effects on electronic bands or Landau-level structure.

4. Local observables in the magnetic-HMO framework

Besides global spectral quantities, the magnetic-HMO formulation provides direct access to local electronic observables through the flux-dependent eigenvectors of the magnetic adjacency matrix $\mathcal{A}(\Phi)$. Let $\psi_n(\Phi)$ denote the normalized eigenvectors of the one-electron Hamiltonian $H(\Phi) = t\,\mathcal{A}(\Phi)$ and f_n the orbital occupations. The one-particle density matrix is

$$\Gamma_{ij}(\Phi) = \sum_n g_n \psi_n(i;\Phi)\psi_n^*(j;\Phi).$$

Accordingly, $\langle c_i^\dagger c_j \rangle = \Gamma_{ji}(\Phi)$. Several physically relevant observables follow directly from $\gamma(\Phi)$.

4.1. Charge density and bond order

The π-electron charge density at site i is

$$\rho_i(\Phi) = \Gamma_{ii}(\Phi),$$

while the (magnetic) bond order between sites i and j is

$$P_{ij}(\Phi) = \Gamma_{ij}(\Phi).$$

At zero flux these reduce to the standard Hückel charge densities and bond orders.

Proposition 4.1 (Basic identities for charge density and bond order)**.** *Let $H(\Phi) = t\,\mathcal{A}(\Phi)$ be the magnetic-HMO one-electron Hamiltonian with eigenpairs $\{E_n(\Phi), \psi_n(\Phi)\}$ and occupations g_n. Define the one-particle density matrix*

$$\gamma(\Phi) = \sum_n f_n\, \psi_n(\Phi)\psi_n(\Phi)^*, \qquad \Gamma_{ij}(\Phi) = \sum_n g_n \psi_n(i;\Phi)\psi_n^*(j;\Phi),$$

so that $\rho_i(\Phi) = \mathit{\Gamma}_{ii}(\Phi)$ and $P_{ij}(\Phi) = \mathit{\Gamma}_{ij}(\Phi)$. Then:

Hermiticity and bounds. *$\gamma(\Phi)$ is Hermitian, hence $P_{ji}(\Phi) = \overline{P_{ij}(\Phi)}$ and $\rho_i(\Phi) \in \mathbb{R}$. Moreover,*

$$0 \le \rho_i(\Phi) \le \max_n g_n, \qquad |P_{ij}(\Phi)|^2 \le \rho_i(\Phi)\,\rho_j(\Phi).$$

Particle-number sum rule.

$$\sum_{\mathrm{i} \in V} \rho_i(\Phi) = \operatorname{Tr}\gamma(\Phi) = \sum_n g_n.$$

In particular, for a closed-shell N-electron system (spin included), $\sum_i \rho_i(\Phi) = N$.

Projector property at $T = 0$***.*** *At zero temperature with closed-shell filling ($g_n \in \{0, 2\}$),*

$$\gamma(\Phi) = 2\, P_{\mathrm{occ}}(\Phi),$$

where $P_{\mathrm{occ}}(\Phi)$ is the orthogonal projector onto the span of the occupied eigenvectors. Consequently,

$$\gamma(\Phi)^2 = 2\,\gamma(\Phi),$$

and all eigenvalues of $\gamma(\Phi)$ are either 0 or 2.

Proof. (1) Since $g_n \in \mathbb{R}$ and $(\psi_n \psi_n^*)^* = \psi_n \psi_n^*$, each rank-one matrix $g_n \psi_n \psi_n^*$ is Hermitian. Therefore, $\Gamma(\Phi)$ is Hermitian, which implies $\Gamma_{ji}(\Phi) = \overline{\Gamma_{ij}(\Phi)}$ and $\rho_i = \Gamma_{ii}(\Phi) \in \mathbb{R}$. Moreover,

$$\rho_i(\Phi) = \sum_n g_n |\psi_n(i;\Phi)|^2 \geq 0.$$

Using completeness

$$\sum_n |\psi_n(i;\Phi)|^2 = 1$$

gives

$$\rho_i(\Phi) \leq \left(\max_n g_n\right) \sum_n |\psi_n(i;\Phi)|^2 = \max_n g_n.$$

□

For the bond-order bound, define

$$a = (\sqrt{g_n}\, \psi_n(i;\Phi))_n, \qquad b = (\sqrt{g_n}\, \psi_n(j;\Phi))_n.$$

Then

$$P_{ij}(\Phi) = \Gamma_{ij}(\Phi) = \sum_n g_n \psi_n(i;\Phi) \psi_n^*(j;\Phi) = b^* a,$$

and

$$\rho_i(\Phi) = \|a\|_2^2, \qquad \rho_j(\Phi) = \|b\|_2^2.$$

By Cauchy–Schwarz,

$$|P_{ij}(\Phi)|^2 = |b^* a|^2 \leq \|a\|_2^2 \|b\|_2^2 = \rho_i(\Phi)\rho_j(\Phi).$$

Remark 4.2. Under a local gauge transformation

$$\psi(i) \mapsto \mathrm{e}^{\mathrm{i}\alpha_i} \psi(i),$$

the density is invariant (ρ_i unchanged), while the bond order transforms as

$$P_{ij} \mapsto \mathrm{e}^{i(\alpha_i - \alpha_j)} P_{ij};$$

hence $|P_{ij}|$ is gauge-invariant.

In the magnetic-HMO model with zero on-site energies and half filling, both the π-electron charge density and the bond orders are obtained from the one-electron density matrix $\gamma(\Phi)$. The site population is given by the diagonal elements

$$\rho_i(\Phi) = \Gamma_{ii}(\Phi) = \sum_{n \in \mathrm{occ}} |\psi_n(i;\Phi)|^2,$$

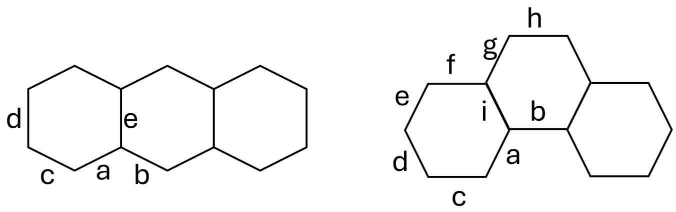

FIGURE 4. Illustration of the bond labels of anthracene (left) and phenanthrene (right).

while the (magnetic) bond order between sites i and j is

$$P_{ij}(\Phi) = \Gamma_{ij}(\Phi) = \sum_{n \in \mathrm{occ}} \psi_n(i; \Phi)\psi_n^*(j; \Phi).$$

For bipartite molecular graphs, the magnetic-HMO Hamiltonian retains the particle--hole symmetry of the HMO model, so the spectrum is symmetric about zero energy. When the Fermi level lies in a spectral gap, the occupied subspace is uniquely defined by the negative-energy eigenstates. In this situation the density matrix is invariant under the symmetries of the molecular graph, and both the site populations and bond orders remain symmetry-consistent.

In a spinless half-filled convention one would obtain $\rho_i = \frac{1}{2}$. However, throughout the present work we use the standard closed-shell spin-included convention, for which $\rho_i = 1$ for neutral alternant hydrocarbons at half filling.

A different situation arises when the magnetic field drives eigenvalues to zero energy so that HOMO = LUMO = 0. In this case the Fermi level lies in a degenerate zero-energy subspace and the occupied subspace is no longer uniquely defined within a closed-shell one-electron description. Any orthonormal basis of the zero-energy eigenspace is admissible, and numerical diagonalization may select different linear combinations of these states. As a consequence, both the site populations $\rho_i(\Phi)$ and the bond orders $P_{ij}(\Phi)$ computed from individual eigenvectors can exhibit apparent flux-dependent variations that depend on how the degeneracy is resolved numerically rather than on a genuine physical charge redistribution or bond-order change.

This situation occurs in anthracene for $f = 0.25$ and $f = 0.5$, where the magnetic-HMO spectrum satisfies HOMO = LUMO = 0. A symmetry-consistent definition of the density matrix is obtained by assigning equal fractional occupation to the zero-energy manifold. If ν denotes the degeneracy of the zero-energy subspace and r the number of electrons to be placed there at half filling, the density matrix can be written as

$$\gamma(\Phi) = \sum_{E_n < 0} |\psi_n\rangle\langle\psi_n| + \frac{r}{\nu} \sum_{E_n = 0} |\psi_n\rangle\langle\psi_n|.$$

This prescription makes the density matrix independent of the particular basis chosen within the degenerate subspace and restores the symmetry- consistent charge density and bond orders expected from the molecular graph.

Example 4.3. We consider the bond orders of the molecules of anthracene and phenanthrene with bonds labeled as indicated in Figure 4.

We compare the flux-dependent bond orders in anthracene and phenanthrene, revealing qualitatively different responses of the π-electron network to the magnetic field. In anthracene, the bond orders at $f = 0.25$ remain approximately proportional to their zero-field values. However, this proportionality is no longer preserved at $f = 0.50$. While at $f = 0$ the largest double-bond character is observed for bond c, at $f = 0.50$ the largest double-bond character shifts to bond d. The central bond e decreases its double-bond character from $f = 0$ to

TABLE 1. Values of the HMO bond orders ($f = 0.0$) for anthracene and phenanthrene using the labeling given in Figure 4, as well as the bond orders obtained from the magnetic-HMO model for $f = 0.25$ and $f = 0.5$. All bond orders are reported in the standard closed-shell spin-included convention, with orbital occupation numbers $g_n = 2$ for occupied orbitals.

	anthracene				phenanthrene		
	f				f		
bond	0.0	0.25	0.50	bond	0.0	0.25	0.50
a	0.606	0.609	0.460	a	0.590	0.615	0.547
b	0.535	0.507	0.536	b	0.460	0.392	0.577
c	0.737	0.755	0.561	c	0.702	0.645	0.356
d	0.586	0.533	0.630	d	0.623	0.640	0.589
e	0.485	0.508	0.331	e	0.707	0.674	0.658
				f	0.575	0.599	0.493
				g	0.506	0.440	0.536
				h	0.775	0.672	0.054
				i	0.542	0.567	0.340

$f = 0.50$. Overall, however, the magnetic field produces only moderate changes in the bond-order distribution in anthracene.

Phenanthrene, by contrast, shows a much clearer redistribution of bond order as the flux increases. At zero field, the strongest double-bond character is found on bond h, followed by bonds c and e, while bond b exhibits the weakest bonding. At $f = 0.50$, the bond-order pattern becomes nearly inverted relative to the zero-field case. The largest double-bond character is now observed for bond e, followed by bonds d and b, which previously displayed the weakest bonding. In contrast, bond h, which initially had the largest double-bond character, loses most of its double-bond signature, with a bond order of only 0.054.

This difference can be understood in terms of molecular topology. Anthracene consists of linearly fused rings that share a single dominant conjugation pathway, so the magnetic perturbation primarily modifies the overall delocalization of electrons along the molecular backbone. Phenanthrene, on the other hand, contains angularly fused rings that create multiple competing conjugation pathways. The magnetic field couples differently to these pathways, producing a redistribution of electronic density and bond order within the π system. The magnetic-HMO density matrix therefore predicts a relatively uniform weakening of bonding in anthracene, but a flux-driven reorganization of bonding in phenanthrene.

4.2. Bond currents

Within the Peierls-substituted Hamiltonian

$$\hat{H}(\Phi) = \sum_{\langle i,j \rangle} t\, \mathrm{e}^{\mathrm{i}\varphi_{ij}(\Phi)} c_i^\dagger c_j + \text{h.c.},$$

the bond-current operator associated with an oriented edge (i, j) is defined as

$$\hat{I}_{ij} := -\frac{\partial \hat{H}}{\partial \varphi_{ij}} = -it \left(\mathrm{e}^{\mathrm{i}\varphi_{ij}} c_i^\dagger c_j - \mathrm{e}^{-i\varphi_{ij}} c_j^\dagger c_i \right).$$

Since φ_{ij} is dimensionless, $\hat{I}_{ij}$ has units of energy; the corresponding physical particle current differs by a factor $1/\hbar$, and the electric current by a factor $q/\hbar$.

With the closed-shell spin-included convention used in this work, its ground-state expectation value is

$$I_{ij}(\Phi) = 4t \sum_{n \in \mathrm{occ}} \Im\big[\mathrm{e}^{\mathrm{i}\varphi_{ij}} \psi_n^*(i;\Phi)\psi_n(j;\Phi)\big] .$$

Equivalently, using the spin-included density-matrix element

$$\Gamma_{ji}(\Phi) = 2 \sum_{n \in \mathrm{occ}} \psi_n^*(i;\Phi)\psi_n(j;\Phi),$$

this can be written as

$$I_{ij}(\Phi) = 2t\, \Im\big[\mathrm{e}^{\mathrm{i}\varphi_{ij}} \Gamma_{ji}(\Phi)\big] .$$

The expression with prefactor $2t$ and a sum over occupied spatial orbitals corresponds to the spinless convention; in the closed-shell convention the additional factor of two accounts for spin degeneracy. Although the Peierls phases depend on the gauge choice, the currents $I_{ij}(\Phi)$ are gauge-invariant observables.

Proposition 4.4. *[Basic properties of bond currents] Consider the Peierls-substituted tight-binding Hamiltonian*

$$\hat{H}(\Phi) = \sum_{\langle i,j \rangle} t\, \mathrm{e}^{\mathrm{i}\varphi_{ij}(\Phi)} c_i^\dagger c_j + \text{h.c.}, \qquad t \in \mathbb{R},$$

with $\varphi_{ji} = -\varphi_{ij}$. For an oriented edge (i,j) define the bond-current operator

$$\hat{I}_{ij} := -\frac{\partial \hat{H}}{\partial \varphi_{ij}} = -\, it \left(\mathrm{e}^{\mathrm{i}\varphi_{ij}} c_i^\dagger c_j - \mathrm{e}^{-i\varphi_{ij}} c_j^\dagger c_i \right),$$

which has units of energy. Since φ_{ij} is dimensionless, $\hat{I}_{ij}$ has units of energy; the corresponding physical particle current differs by a factor $1/\hbar$, and the electric current by a factor $q/\hbar$.

Let $\{\psi_n(\Phi)\}$ be the normalized eigenvectors of the one-electron Hamiltonian

$$H(\Phi) = t\, \mathcal{A}(\Phi),$$

and let the many-electron ground state be obtained by occupying the orbitals in a closed shell (spin included). Then the ground-state bond current is

$$I_{ij}(\Phi) := \langle \hat{I}_{ij} \rangle = 4t \sum_{n \in \mathrm{occ}} \Im\Big[\mathrm{e}^{\mathrm{i}\varphi_{ij}(\Phi)} \psi_n^*(i;\Phi)\psi_n(j;\Phi)\Big] .$$

Moreover:

Antisymmetry.

$$I_{ji}(\Phi) = -I_{ij}(\Phi).$$

Continuity (Kirchhoff law). *For every vertex i,*

$$\sum_{j\colon \{i,j\} \in E} I_{ij}(\Phi) = 0,$$

i.e. the net current leaving i vanishes in any stationary eigenstate and hence in the ground state.

Gauge invariance. *Under a local gauge transformation*

$$c_i \mapsto \mathrm{e}^{\mathrm{i}\alpha_i} c_i, \qquad \varphi_{ij} \mapsto \varphi_{ij} + (\alpha_i - \alpha_j),$$

the expectation values $I_{ij}(\Phi)$ are unchanged.

Proof. Proof. First, differentiating $\hat{H}(\Phi)$ with respect to φ_{ij} gives

$$-\frac{\partial}{\partial \varphi_{ij}} \left(t\, \mathrm{e}^{\mathrm{i}\varphi_{ij}} c_i^\dagger c_j + t\, \mathrm{e}^{-i\varphi_{ij}} c_j^\dagger c_i \right) = -\, it \left(\mathrm{e}^{\mathrm{i}\varphi_{ij}} c_i^\dagger c_j - \mathrm{e}^{-i\varphi_{ij}} c_j^\dagger c_i \right),$$

which is the stated operator $\hat{I}_{ij}$.

For the expectation value, note that in a Slater determinant (closed shell) the one-particle density matrix satisfies

$$\Gamma_{ji}(\Phi) = 2 \sum_{n \in \mathrm{occ}} \psi_n^*(i;\Phi)\psi_n(j;\Phi),$$

and

$$\langle c_i^\dagger c_j \rangle = \Gamma_{ji}(\Phi).$$

Therefore,

$$\begin{aligned}
I_{ij}(\Phi) &= \langle \hat{I}_{ij} \rangle \\
&= -\, it \left(\mathrm{e}^{\mathrm{i}\varphi_{ij}} \langle c_i^\dagger c_j \rangle - \mathrm{e}^{-i\varphi_{ij}} \langle c_j^\dagger c_i \rangle \right) \\
&= -\, it \left(\mathrm{e}^{\mathrm{i}\varphi_{ij}} \Gamma_{ji} - \mathrm{e}^{-i\varphi_{ij}} \overline{\Gamma_{ji}} \right) \\
&= 2t\, \Im\!\left(\mathrm{e}^{\mathrm{i}\varphi_{ij}} \Gamma_{ji} \right) \\
&= 4t \sum_{n \in \mathrm{occ}} \Im\!\left[\mathrm{e}^{\mathrm{i}\varphi_{ij}} \psi_n^*(i;\Phi)\psi_n(j;\Phi) \right],
\end{aligned}$$

as claimed.

(1) Using $\varphi_{ji} = -\varphi_{ij}$ and swapping i and j,

$$\begin{aligned}
I_{ji}(\Phi) &= 4t \sum_{n \in \mathrm{occ}} \Im\!\left[\mathrm{e}^{\mathrm{i}\varphi_{ji}} \psi_n^*(j)\psi_n(i) \right] \\
&= 4t \sum_{n \in \mathrm{occ}} \Im\!\left[\overline{\mathrm{e}^{\mathrm{i}\varphi_{ij}} \psi_n^*(i)\psi_n(j)} \right] \\
&= -\, I_{ij}(\Phi),
\end{aligned}$$

since $\Im(\overline{z}) = -\Im(z)$.

(2) Let $|\Psi\rangle$ be any stationary many-electron state of $\hat{H}(\Phi)$ (*e.g.* an eigenstate, including the ground state). The number operator at site i is

$$\hat{n}_i = c_i^\dagger c_i.$$

Using the Heisenberg equation,

$$\frac{\mathrm{d}}{\mathrm{d}t}\langle \hat{n}_i \rangle = \frac{i}{\hbar}\langle [\hat{H}(\Phi), \hat{n}_i] \rangle.$$

A direct commutator calculation shows that

$$\frac{i}{\hbar}[\hat{H}(\Phi), \hat{n}_i] = \frac{1}{\hbar}\sum_{j:\{i,j\}\in E} \hat{I}_{ij},$$

so stationarity implies

$$\frac{\mathrm{d}}{\mathrm{d}t}\langle \hat{n}_i \rangle = 0$$

and hence

$$\sum_j \langle \hat{I}_{ij} \rangle = 0,$$

i.e.

$$\sum_j I_{ij}(\Phi) = 0.$$

(3) Under the local gauge transformation

$$c_i \mapsto \mathrm{e}^{\mathrm{i}\alpha_i} c_i$$

one has

$$c_i^\dagger c_j \mapsto \mathrm{e}^{-i\alpha_i}\mathrm{e}^{\mathrm{i}\alpha_j} c_i^\dagger c_j,$$

while the Peierls phase shifts as

$$\varphi_{ij} \mapsto \varphi_{ij} + (\alpha_i - \alpha_j).$$

Hence

$$\mathrm{e}^{\mathrm{i}\varphi_{ij}} c_i^\dagger c_j \mapsto \mathrm{e}^{i(\varphi_{ij}+\alpha_i-\alpha_j)}\mathrm{e}^{-i\alpha_i}\mathrm{e}^{\mathrm{i}\alpha_j} c_i^\dagger c_j = \mathrm{e}^{\mathrm{i}\varphi_{ij}} c_i^\dagger c_j,$$

and similarly for its Hermitian conjugate. Therefore $\hat{H}(\Phi)$ and $\hat{I}_{ij}$ are gauge-invariant operators, and so are their expectation values $I_{ij}(\Phi)$. □

Example 4.5. We consider three pairs of molecules for which bond currents are computed and compared at $f = 0.25$ (see Fig. 5): naphthalene (I) and chrysene (II); anthracene (III) and phenanthrene (IV); triphenylene (V) and coronene (VI). In naphthalene, the bond-current pattern shows a dominant circulation along the ten-membered peripheral cycle, with almost no participation of the central C–C bond connecting the two benzene rings. When two additional hexagons are fused to naphthalene to form chrysene, the largest bond currents shift toward the outer rings of the molecule. Although a circulation is still present in the bonds belonging to the two central rings, its magnitude is clearly smaller than that observed along the external perimeter.

The comparison between anthracene and phenanthrene highlights the effect of molecular topology. In the linear acene anthracene, the current is mainly concentrated on the bonds of the two terminal rings and on the two inter-ring bonds along the molecular backbone, while the remaining bonds of the central ring carry almost no current. In contrast, in the angularly fused phenanthrene molecule the current is redistributed toward the central ring, with only weak currents flowing along the peripheral bonds. This reflects the different conjugation pathways available in linear and angular ring fusion.

A similar contrast appears in the pair triphenylene and coronene. In triphenylene, bond currents are largely localized in the three peripheral benzene rings, while the central ring carries almost no current, except along the bonds that fuse adjacent rings. In coronene, however, the current pattern is qualitatively different: a strong circulation develops in the central ring, accompanied by a peripheral current distributed along the bonds of the eighteen-membered outer cycle.

These examples illustrate how magnetic-field-induced bond currents are strongly influenced by molecular topology and by the availability of competing conjugation pathways, leading to distinct circulation patterns even among structurally related polyaromatic hydrocarbons.

4.3. Ring currents

For a face $\mathscr{F}$ of the molecular graph, the net ring current is defined as the oriented sum of bond currents along its boundary,

$$I_{\mathscr{F}}(\Phi) = \sum_{(i \to j) \in \partial \mathscr{F}} I_{ij}(\Phi).$$

These quantities characterize the local circulation of π-electron currents induced by the magnetic field.

Proposition 4.6 (Ring (face) currents)**.** *Let $G = (V, E)$ be a planar embedding of the molecular graph, and let $\mathscr{F}$ be a face with oriented boundary $\partial \mathscr{F}$ (a directed cycle) consistent with a chosen orientation (e.g. counterclockwise). Given bond currents $I_{ij}(\Phi)$ on oriented edges (as in Prop. 4.4), define the ring current around f by*

$$I_{\mathscr{F}}(\Phi) \coloneqq \sum_{(i \to j) \in \partial f} I_{ij}(\Phi).$$

Then:

Orientation dependence. *Reversing the orientation of $\partial \mathscr{F}$ changes the sign: if $\partial \mathscr{F}$ is traversed in the opposite direction, then $I_{\mathscr{F}}(\Phi)$ is replaced by $-I_{\mathscr{F}}(\Phi)$.*

Gauge invariance. *$I_{\mathscr{F}}(\Phi)$ is gauge invariant.*

Flux sensitivity. *If Φ is gauge-trivial on $\partial \mathscr{F}$ (i.e. the total Peierls phase around $\partial \mathscr{F}$ is 0 modulo 2π), then $I_{\mathscr{F}}(\Phi) = 0$ for any time-reversal-symmetric filling (in particular at $\Phi = 0$).*

Proof. 1) If the boundary orientation is reversed, every directed edge $(i \to j)$ on $\partial \mathscr{F}$ is replaced by $(j \to i)$, and by antisymmetry of bond currents (Prop. 4.4), $I_{ji}(\Phi) = -I_{ij}(\Phi)$, hence the sum changes sign.

(2) Each bond current $I_{ij}(\Phi)$ is gauge invariant by Proposition 4.4; therefore any finite sum of such currents, in particular $I_{\mathscr{F}}(\Phi)$, is gauge invariant.

(3) If the total Peierls phase around $\partial \mathscr{F}$ vanishes modulo 2π, then the restriction of the magnetic adjacency to that cycle is unitarily gauge-equivalent to the zero-field adjacency on the same cycle (cycle-triviality). At $\Phi = 0$, time-reversal symmetry implies vanishing bond currents and hence $I_{\mathscr{F}}(0) = 0$. More generally, for a time-reversal-symmetric filling, reversing the flux changes the sign of all bond currents, so $I_{\mathscr{F}}(\Phi)$ is odd under $\Phi \mapsto -\Phi$ and in particular vanishes when the effective flux through $\mathscr{F}$ is zero. $\square$

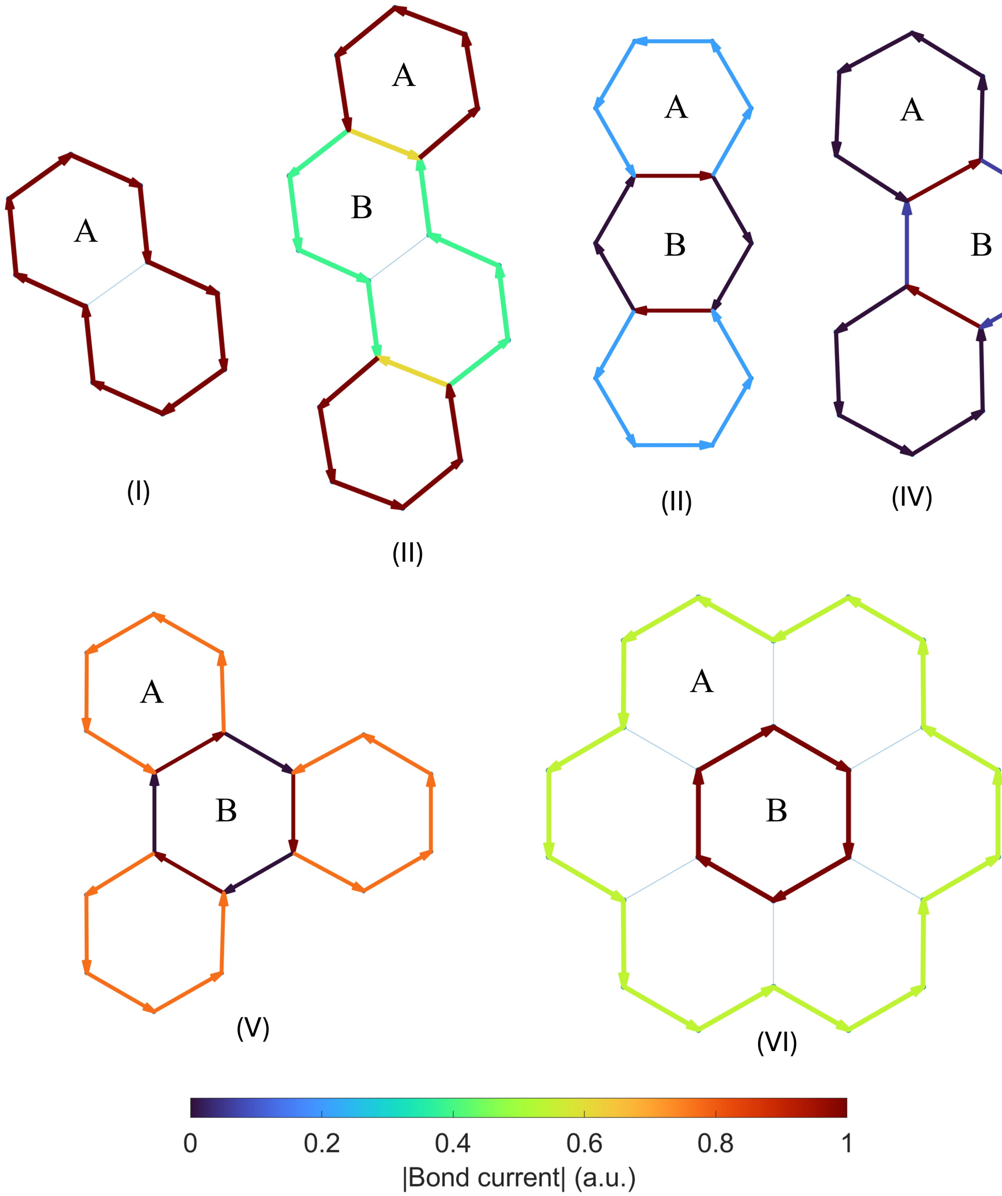

FIGURE 5. Magnetic current at each bond of three pairs of polycyclic aromatic hydrocarbons studied in this work. The calculations are for $f = 0.25$. The molecules are: naphthalene (I) and chrysene (II); anthracene (III) and phenanthrene (IV); triphenylene (V) and coronene (VI).

Example 4.7. We consider here the ring currents of the six molecules illustrated in Figure 5. The calculated values for the rings marked in that figure are reported in Table 2.

In most of the molecules examined, the outermost and innermost rings support currents flowing in opposite directions. In the present sign convention, the peripheral rings display negative ring currents, while the most internal rings exhibit positive ring currents. This counter-rotating pattern appears clearly in naphthalene, anthracene, phenanthrene, triphenylene, and coronene. The only exception among the molecules considered here

TABLE 2. Ring currents $I_f(\Phi) \cdot 10^2$ for the rings A and B of the six molecules illustrated in Figure 5.

	I	II	III	IV	V	VI
A	3.88	−3.57	−4.26	−3.04	−4.48	−2.48
B		−0.59	4.23	3.61	3.13	5.66

is the zigzag-fused structure of chrysene, where the redistribution of current among the rings does not produce a simple outer-versus-inner opposition.

This behavior reflects the competition between global and local circulation pathways in polyaromatic hydrocarbons under a magnetic perturbation. The external perimeter of the molecule often supports a dominant global circulation pathway, while inner rings may sustain secondary currents that respond differently to the magnetic field. As a result, opposite ring-current directions can arise naturally between the outer boundary of the π system and its internal rings.

The effect is particularly evident in molecules with concentric or quasi-concentric conjugation pathways, such as triphenylene and coronene, where the coexistence of peripheral and internal circulation channels leads to counter-rotating ring currents. In contrast, in chrysene the zigzag fusion of rings modifies the connectivity of the π network and alters the balance between local and global current pathways, preventing the emergence of a clear inner–outer opposition.

Overall, the ring-current patterns illustrate how magnetic-field-induced π circulation depends sensitively on molecular topology and on the interplay between local aromatic circuits and larger conjugated pathways.

5. Magnetic-HMO in perspective

Although the present work focuses on finite conjugated hydrocarbons, the magnetic-HMO construction is not restricted to the small molecular examples considered here. In principle, the method extends to larger conjugated systems by diagonalizing the corresponding magnetic adjacency Hamiltonian, with the main numerical limitation being the size of the Hermitian matrix. For large sparse systems, standard sparse eigensolvers may be used when only the occupied states or the states near the Fermi level are required [40]. The same framework could also be adapted to extended conjugated materials, including covalent organic frameworks or metal--organic frameworks with well-defined π-conjugated pathways [41, 42], provided that an appropriate effective orbital basis and hopping parametrization are available.

More generally, the Peierls-phase construction is not limited to cyclic molecules: for an embedded molecular graph, magnetic phases can be assigned from the line integral of the vector potential along each bond [33, 34]. Thus, non-cyclic and non-planar geometries can also be considered, although the interpretation of local ring fluxes becomes geometry--dependent. Finally, the present magnetic-HMO model should be viewed as a transparent graph-theoretical and tight-binding-level framework that complements DFT, ab initio, and modern effective-Hamiltonian approaches, rather than as a replacement for them. In particular, the model may provide qualitative and topology-based insight into magnetic response, orbital-current organization, and flux-dependent spectral rearrangements in conjugated systems. Because the formulation is based on a Hermitian tight-binding Hamiltonian with Peierls phases, it is also compatible in spirit with current ab initio-derived tight-binding approaches [43, 44] and with effective lattice Hamiltonians used in quantum simulation and quantum-computing implementations of molecular electronic structure [45, 46]. In this sense, the magnetic-HMO framework may be useful both as an interpretable reduced model and as a conceptual bridge between graph-theoretical descriptions and higher-level electronic-structure methodologies.

6. Computational methods

All calculations were performed using an in-house MATLAB implementation of the magnetic HMO method. Molecular structures were defined either by explicit adjacency matrices or by Cartesian coordinates obtained

TABLE 3. Parameters used in the calculations with the magnetic-HMO method.

Quantity / procedure	Implementation used in this work
Construction of adjacency matrices	For calculations based on Cartesian coordinates, two carbon atoms were connected whenever their Euclidean distance satisfied $d_{ij} < 1.7$. For several benchmark systems (*e.g.* benzene and idealized cycles), adjacency matrices were defined explicitly.
Gauge choice	Symmetric gauge: $\mathbf{A}(\mathbf{r}) = \frac{1}{2}\mathbf{B} \times \mathbf{r}$. The magnetic field was taken perpendicular to the molecular plane.
Peierls phase assignment	For a bond connecting sites i and j with Cartesian coordinates (x_i, y_i) and (x_j, y_j), the Peierls phase was computed as $\phi_{ij} = \frac{\pi f}{A_{\text{ref}}}(x_i y_j - x_j y_i)$, corresponding to the straight-line Peierls integral in the symmetric gauge.
Flux normalization	The reduced flux was defined as $f = \Phi/\Phi_0$. For polycyclic systems, the normalization area was chosen as the median bounded-face area: $A_{\text{ref}} = \text{median(areas)}$. Thus f corresponds to the flux through a reference hexagonal face.
Phase assignment in polycyclic systems	The same symmetric-gauge Peierls prescription was applied consistently to every bond of the molecular graph using the Cartesian coordinates of the corresponding carbon atoms.
DOS broadening	Gaussian broadening with parameter $\eta = 0.1\|\beta\|$.
Energy grid for DOS	1500 uniformly spaced energy points between the minimum eigenvalue minus 0.5 and the maximum eigenvalue plus 0.5.
Flux grids	Unless otherwise stated, calculations used uniformly spaced grids in $f \in [0, 1]$ with either 201, 401, or 501 points depending on the calculation.
Magnetization calculation	The orbital magnetization was computed numerically using MATLAB finite-difference differentiation (`gradient`).
Susceptibility calculation	The orbital susceptibility was computed from local quadratic fitting of the ground-state energy: $E_{\text{GS}}(f) \simeq af^2 + bf + c$, $\chi(f) = -2a$. A moving fitting window with $2 \times 7 + 1$ flux points was used.
Occupation convention	Closed-shell occupation of the lowest-energy orbitals after eigenvalue sorting.
Treatment of degeneracies	When the Fermi level lies inside a degenerate manifold, fractional occupation of the degenerate orbitals was used.
Ring-cycle detection	Ring cycles were detected automatically from the planar molecular graph using the face structure returned by the cycle-detection routines in the magnetic-HMO implementation.

Table 3. Continued.

Ring-current definition	Ring currents were computed as averages of the oriented bond currents around the boundary of each face.
Bond-current normalization	Bond currents and ring currents are reported in dimensionless units proportional to the hopping amplitude $\lvert t\rvert$. Closed-shell spin degeneracy was included consistently throughout the calculations.
Software	All calculations were performed in MATLAB using original codes developed by the author and given in a Supplementary Information to this paper.

from the IQmol molecular fragment library for polyaromatic hydrocarbons, available from the IQmol GitHub repository [47]. When Cartesian coordinates were used as input, the corresponding molecular graph was constructed automatically from the carbon-atom connectivity.

For each value of the reduced magnetic flux, the complex magnetic-HMO Hamiltonian was diagonalized numerically to obtain the eigenvalues and eigenvectors. Ground-state energies were computed within the closed-shell approximation by occupying the lowest-energy molecular orbitals. The one-particle density matrix was then constructed from the occupied eigenvectors, from which atomic charge densities and bond orders were obtained. Bond currents were evaluated from the field-dependent Hamiltonian and density matrix using the magnetic-HMO current operator, while ring currents were obtained from the corresponding oriented bond currents around the molecular cycles.

Density-of-states (DOS) curves were obtained from Gaussian broadening of the discrete magnetic-HMO eigenvalues. Orbital magnetization and orbital susceptibility were computed numerically from the flux dependence of the ground-state energy. Bond-current maps and ring-current visualizations were generated directly on the molecular connectivity graph using the projected Cartesian coordinates.

All quantities reported in this work are expressed in units of the HMO resonance integral β, with $\beta = -1$. The principal numerical parameters and computational conventions used throughout the work are summarized in Table 3.

Conclusions

We have developed a magnetic extension of the Hückel molecular orbital method in which Peierls phase factors incorporate the effect of an external magnetic field into the π-electron Hamiltonian of a conjugated molecule. Within this framework, the Hamiltonian of the magnetic-HMO model is naturally represented as a complex-weighted hopping operator on the hydrogen-depleted molecular graph. Under the usual Hückel assumptions, the corresponding one-electron magnetic-HMO Hamiltonian is proportional to the Hermitian adjacency matrix, providing a direct physical interpretation of this matrix within molecular electronic structure theory.

The magnetic-HMO formulation enables the computation of global flux-dependent observables such as orbital magnetization and orbital susceptibility from the flux-dependent magnetic adjacency spectrum, while local observables such as bond currents and ring currents are determined by the corresponding eigenvectors or one-particle density matrix. Numerical results for several polycyclic aromatic hydrocarbons show that the magnetic response of π-electron systems depends strongly on the topology of the molecular graph. Linear acenes exhibit a regular zigzag structure in the orbital magnetization as a function of the reduced flux, whereas nonlinear and extended polycyclic systems show less regular oscillatory behavior arising from the presence of multiple conjugation pathways.

The oscillatory magnetic response predicted by the magnetic-HMO model originates from flux-dependent rearrangements of discrete molecular energy levels and provides a finite-molecule analogue of magnetic oscillations observed in Peierls-phase tight-binding systems. More generally, the magnetic-HMO method establishes a bridge between Hückel theory, Hermitian graph operators, and magnetic tight-binding models. This connection opens new perspectives for studying topology-dependent magnetic phenomena in conjugated molecules and for exploring flux-dependent spectral and electronic properties of molecular graphs.

Acknowledgments

I sincerely thank the reviewers for their careful reading of the manuscript and for their insightful comments and constructive suggestions, which have significantly improved the clarity, rigor, and overall presentation of the paper. The author also thanks financial support from Agencia Estatal de Investigación (AEI, MCI, Spain) MCIN/AEI/ 10.13039/501100011033 under grant PID2023-149473NB-I00 and by Agencia Estatal de Investigación (AEI, MCI, Spain) MCIN/AEI/ 10.13039/501100011033 and Fondo Europeo de Desarrollo Regional (FEDER, UE) under the María de Maeztu Program for units of Excellence in R&D, grant CEX2021-001164-M).

Conflicts of interest

The author declares that he has no conflict of interest.

Data availability statement

Data used in this article is publicly available at the repository indicated in the paper.

Author contribution statement

Ernesto Estrada: investigation, writing – original draft, methodology, coding, validation, visualization.

References

[1] A.T. Balaban, editor. Chemical Applications of Graph Theory. Academic Press (1985).

[2] C.A. Coulson, On the calculation of the energy in unsaturated hydrocarbon molecules. *Proc. Cambr. Philos. Soc.* **36** (1940) 201–203.

[3] D. Cvetković, M. Doob and H. Sachs, Spectra of Graphs. Johann Ambrosius Barth (1995).

[4] I. Gutman and O.E. Polansky, Mathematical Concepts in Organic Chemistry. Springer Science & Business Media (2012).

[5] E. Huckel, Quantentheoretische beiträge zum benzolproblem. zum bezolproblem, quantentheoretische beiträge and zum problem, quantentheoretische beiträge. *Z. Phys. Chem.* **70** (1931) 204–286.

[6] J.C. Slater and G.F. Koster, Simplified LCAO method for the periodic potential problem. *Phys. Rev.* **94** (1954) 1498.

[7] T.B. Boykin, Recent developments in tight-binding approaches for nanowires. *J. Computat. Electron.* **8** (2009) 142–152.

[8] S. Schulz and G.J.P.R.B. Czycholl, Tight-binding model for semiconductor nanostructures. *Phys. Rev. B Condensed Matter Mater. Phys.* **72** (2005) 165317.

[9] J.S. Fabila-Carrasco, F. Lledó and O. Post, Matching number, Hamiltonian graphs and magnetic Laplacian matrices. *Linear Algebra Appl.* **642** (2022) 86–100.

[10] M. Fanuel, C.M. Alaíz, Á. Fernández and J.A.K. Suykens, Magnetic eigenmaps for the visualization of directed networks. *Appl. Computat. Harmonic Anal.* **44** (2018) 189–199.

[11] M. Fanuel and J. Suykens, Magnetic Laplacian for directed graphs. *Appl. Computat. Harmonic Anal.* **40** (2016) 469–509.

[12] S. Furutani, T. Shibahara, M. Akiyama, K. Hato and M. Aida, Graph signal processing for directed graphs based on the Hermitian Laplacian, in *Joint European Conference on Machine Learning and Knowledge Discovery in Databases*. Springer (2019) 447–463.

[13] Y. He, M. Perlmutter, G. Reinert and M. Cucuringu, Msgnn: a spectral graph neural network based on a novel magnetic signed Laplacian, in *Learning on Graphs Conference*. PMLR (2022) 40–41.

[14] M. Shubin, Discrete magnetic Laplacian. *Commun. Math. Phys.* **164** (1994) 259–275.
[15] N. Konno, Quantum walks. *Lect. Notes Math.* **1954** (2008) 309–452.
[16] M. Kotani and T. Sunada, Zeta functions of finite graphs. *J. Math. Sci.* **7** (2000) 7–25.
[17] X. Liu and Y. Li, Hermitian-adjacency matrices and hermitian energies of mixed graphs. *Linear Algebra Appl.* **466** (2015) 182–207.
[18] K. Guo and B. Mohar, Hermitian adjacency matrix of digraphs and mixed graphs. *J. Graph Theory* **85** (2017) 217–248.
[19] B. Hoser and A. Geyer-Schulz, Eigenspectral analysis of Hermitian adjacency matrices for the analysis of group substructures. *J. Math. Sociol.* **29** (2005) 265–294.
[20] B. Mohar, A new kind of Hermitian matrices for digraphs. *Linear Algebra Appl.* **584** (2020) 343–352.
[21] M. Abudayah, O. Alomari and O. AbuGhneim, Inverse of Hermitian adjacency matrix of a mixed graph. *Appl. Math. Inf. Sci.* **16** (2022) 823–828.
[22] N. Athmouni, H. Baloudi, M. Damak and M. Ennaceur, The magnetic discrete Laplacian inferred from the Gauß–Bonnet operator and application. *Ann. Funct. Anal.* **12** (2021) 33.
[23] M. Cucuringu, H. Li, H. Sun and L. Zanetti, Hermitian matrices for clustering directed graphs: insights and applications, in *International Conference on Artificial Intelligence and Statistics*. PMLR (2020) 983–992.
[24] A. Jahanbani, On the Hermitian Estrada index of mixed graphs. *Int. J. Appl. Graph Theory* **3** (2019) 14–28.
[25] Y. Ji, W. Wang and H. Zhang, Mixed graphs determined by their generalized Hermitian adjacency spectrum based on Eisenstein integers. *Electron. J. Combinatorics* **32** (2025) 1–56.
[26] S. Kubota, E. Segawa and T. Taniguchi, Quantum walks defined by digraphs and generalized Hermitian adjacency matrices. *Quant. Inform. Process.* **20** (2021) 95.
[27] H. Li and T. Yu, Hermitian adjacency spectrum of Cayley digraphs over dihedral group, in *Algebra Colloquium*, vol. 27. World Scientific (2020) 121–130.
[28] S. Li and Y. Yu, Hermitian adjacency matrix of the second kind for mixed graphs. *Discrete Math.* **345** (2022) 112798.
[29] B. Mohar, Hermitian adjacency spectrum and switching equivalence of mixed graphs. *Linear Algebra Appl.* **489** (2016) 324–340.
[30] T. Peron, B.M.F. de Resende, F.A. Rodrigues, L. da F. Costa and J.A. Méndez-Bermúdez, Spacing ratio characterization of the spectra of directed random networks. *Phys. Rev. E* **102** (2020) 062305.
[31] J. Sanchez, R. Caire and N. Hadjsaid, Application of Hermitian adjacency matrices for the vulnerability analysis of power systems. *IEEE PES ISGT Europe* (2013).
[32] Z. Wang, T. She and C. Wang, The index weighted Hermitian adjacency matrices for mixed graphs. *Utilitas Math.* **119** (2024) 63–71.
[33] R. Peierls, Zur theorie des diamagnetismus von leitungselektronen. *Z. Phys.* **80** (1933) 763–791.
[34] D.R. Hofstadter, Energy levels and wave functions of bloch electrons in rational and irrational magnetic fields. *Phys. Rev. B* **14** (1976) 2239–2249.
[35] I. Gutman, The energy of a graph. *Berichte Math.-Stat. Sektion Forsch. Graz* **103** (1978) 1–22.
[36] I. Gutman and X. Li, Graph Energy. Springer (2012).
[37] E. Estrada and M. Benzi, What is the graph energy? *Linear Algebra Appl.* **544** (2018) 1–17.
[38] Y. Huang, D.F. Gleich and P. Li, Powers of magnetic graph matrix: Fourier spectrum, walk compression, and applications. arXiv preprint arXiv:2506.07343 (2025).
[39] K. Kishigi and Y. Hasegawa, Quantum oscillations of magnetization in tight-binding electrons on a honeycomb lattice. *Phys. Rev. B* **90** (2014) 085427.
[40] Y. Saad, *Numerical Methods for Large Eigenvalue Problems*. SIAM (2011).
[41] Y. Cui, *et al.*, Electrically conductive two-dimensional metal–organic frameworks. *Nat. Commun.* **7** (2016) 10466.
[42] M. Ko, L. Mendecki and K.A. Mirica, Conductive two-dimensional metal–organic frameworks: design, synthesis, and applications. *Chem. Commun.* **54** (2018) 7873–7891.
[43] A.P. Horsfield and A.M. Bratkovsky, Ab initio tight binding. *J. Phys. Condensed Matter* **12** (2000) R1–R24.
[44] F. Liu, M.R. Press, S.N. Khanna and P. Jena, Magnetism and local order: ab initio tight-binding theory. *Phys. Rev. B* **39** (1989) 6914.

[45] Y. Cao, J. Romero, J.P. Olson, *et al.*, Quantum chemistry in the age of quantum computing. *Chem. Rev.* **119** (2019) 10856–10915.

[46] S. McArdle, S. Endo, A. Aspuru-Guzik, S.C. Benjamin and X. Yuan, Quantum computational chemistry. *Rev. Mod. Phys.* **92** (2020) 015003.

[47] IQmol Project Contributors, Polyaromatic hydrocarbon molecular coordinates. https://github.com/nutjunkie/IQmol/tree/master/share/fragments/Molecules/Polyaromatic_Hydrocarbons (2026). Accessed: 2026-02-12.